THE THERMOCHEMICAL ANALYSIS OF POTASSIC-CHLORO-HASTINGSITE AND THE COMPUTATION OF CL-BRINE CONCENTRATIONS IN GNEISSES IN THE BLACK ROCK FOREST, CORNWALL, NY

BY

MONICA WALTON

B.S., State University at Oneonta, 2016

Submitted in partial fulfillment of the requirements for
the degree of Master of Science in Geology
in the Graduate School of
Binghamton University
State University of New York
2021

©Copyright by Monica Anne Walton 2021

All Rights Reserved

Accepted in partial fulfillment of the requirements for
the degree of Master's of Science in Geology
in the Graduate School of
Binghamton University
2021

June 18, 2021

Dr. David Jenkins, Chair and Faculty Advisor
Department of Geological Sciences, Binghamton University

Dr. Tim K. Lowenstein, Member
Department of Geological Sciences, Binghamton University

Dr. Richard Naslund, Member
Department of Geological Sciences, Binghamton University

Abstract:

Cl-rich amphiboles and their interaction with fluids has been a topic of interest for many years. Currently there is very little data on Cl-rich amphiboles, which this study is determined to remedy. The derivation of the thermodynamic data needed in this study started with making as pure a yield of Cl-rich synthetic amphibole with a bulk composition of potassic-chloro-hastingsite ($KCa_2(Fe_4Fe^{3+})(Al_2Si_6)O_{22}Cl_2$= KCH) as possible. About 90-100 mg of sample were treated at a time in either a cold-seal or gas pressure vessel. These were heated to 600-700°, 2-3.5 kbars, and with an oxygen fugacity near NiNiO. After about 2-7 days each sample was extracted and soaked for an additional 2 days to remove any unreacted and soluble salts for mass balance determination. Finally, the phases in each sample were analyzed with the electron microprobe.

These samples were combined and differential scanning calorimetry (DSC) was used to directly measure their heat capacity. The following Cp expression was adopted: Cp ($kJ/K \cdot mol$) = $1.29 + 2.9992x10^{-5}T - 8447.5/T^2 - 8.947/T^{1/2}$. The unit-cell volume of KCH was determined through Rietveld refinements of powder diffraction data from this study and those of Matteucci (2019, MS Thesis) to be 960.6 A^3, or a molar volume of 289.2 cm^3/mol. With all this data and the experimentally determined breakdown boundary of potassic-chloro-hastingsitic amphibole from Matteucci (2019), an enthalpy of formation and third-law entropy at 298K and 1 bar were derived to be ΔH_f = -10,653.57 ± 7 kJ/mol and $S°$= 756.62 ± 6 J/Kmol.

These newly derived thermochemical data for potassic-chloro- hastingsite were then used to understand fluid-rock interactions that formed the Cl-bearing amphiboles in the gneisses of the Black Rock Forest, Cornwall, NY. This involved taking samples from gneisses in the Black Rock Forest in Cornwall, NY and analyzing them for all the mineral phases. These phases include amphibole, quartz, clinopyroxene, orthopyroxene, plagioclase, and/or K-spar. From the mineral assemblages multiple balanced reactions were proposed to come up with the Cl molality (mCl) of the fluids that formed this region. The mCl ranged from 0.20-36.4 over all 4 sampling localities. There was no obvious spatial trend to these molalities suggesting the presence of localized heterogeneity of these metamorphic fluids.

Acknowledgements:

I am grateful for partial support for this study from the NSF grant EAR-1725053 to David M. Jenkins. I am also thankful to the Eastern Federation of Mineralogical and Lapidary Societies for partial support as well.

Huge thanks to William Schuster for showing us around the Black Rock Forest and letting us take samples from there.

I would like to thank Professor David Jenkins for his incredible patience and knowledge in helping me work through this research. Thank you to all of my committee as well, Professor Tim Lowenstein and Professor Richard Naslund for their support.

Lastly, I would like to thank my wonderful fiancée Garret Shaw and all my friends that I have met at Binghamton University.

Table of Contents

List of Tables ---------- viii

List of Figures ---------- ix

1. Introduction ---------- 3
2. Methods ---------- 6
3. Results ---------- 13
4. Discussion ---------- 34
5. Conclusion ---------- 64

References ---------- 66

List of Tables

Table 1: Conditions and products of the amphibole syntheses comprising KHAST-1 ...14

Table 2: Microprobe analyses of each sample 15

Table 3: Mass balance assessment for amphibole synthesis experiments 16

Table 4. Hedenbergite produced in reaction (3) 30

Table 5: Reaction-reversal data used for calculating G' at P and T 32

Table 6: Thermochemical data of K-Cl hastingsite derived and adopted in this study ...33

Table 7: Minerals found in each rock sample indicated by x 36

Table 8 Microprobe Analyses of K-spar.....40

Table 9: Microprobe Analyses of Plagioclase in the Black Rock Forest 42

Table 10: Microprobe Analyses of Clinopyroxene.....45

Table 11: Microprobe Analyses of Orthopyroxene 47

Table 12: Microprobe analyses of magnetite.....48

Table 13: Microprobe Analyses of Amphibole in the Black Rock Forest.....49

Table 14: Activities and molalities derived for the Black Rock Forest.....61

List of Figures

Figure 1. Locations of Samples found in the Black Rock Forest 12

Figure 2: Mass-balance assessment of the amphibole synthesis products from this study 17

Figure 3: FTIR analysis of synthetic pargasite (black curve) and KHAST-1-FM (red curve) in the OH-stretching range.....19

Figure 4: OH stretching region of KHAST-1-FM 19

Figure 5: Thermal scans of synthetic K-Cl-hastingsite (KHAST-1-FM) 21

Figure 6: Cp Tremolite from DSC measurements compared to Holland and Powell, 2011 Cp data 22

Figure 7: Raw Cp (J/K·mol) data for both KHAST-1 and Tremolite.....23

Figure 8. Selected DSC data for natural tremolite matching the published Cp expression of Holland and Powell (2011, HP 2011).....23

Figure 9: Synthetic amphibole (KHAST-1-FM) Cp data from this study (circles) modeled after the ferroactinolite Cp curve from Holland and Powell (2011), giving the Cp curve used in this study (solid black).....24

Figure 10: Volumes of synthetic K-Cl hastingsitic amphiboles with Cl amounts of 0 – 1.7 apfu from this study (star) and Matteucci, 2019 (circles).....27

Figure 11: Thermal stability field of synthetic K-Cl hastingsitic amphibole (Amph).....29

Figure 12: Oxygen fugacity (Frost, 1991) 31

Figure 13. Graph of G' values plotted against temperature and fit with a straight line to determine enthalpy and entropy.....32

Figure 14: Thermal Stability of K-Cl hastingsite 34

Figure 15: Ternary diagram of feldspars found in four different locations in the Black Rock Forest 56

Figure 16: Ternary diagram of pyroxenes found in 4 different locations in the Black Rock Forest.....57

Figure 17: Plots of X_{Si}, X_{Fe2+}, and X_K compared to Cl apfu by location.....58

Figure 18: Cl brine concentrations from the Black Rock Forest superimposed on concentrations of metals in fluids (Yardley, 2005)..... 59

Figure 19: Geologic map of the Black Rock Forest Area with corresponding molalities of $FeCl_2$ to each location. Location 3 was an amalgamation of $CaCl_2$ and FeCl2.....6

1. Introduction:

Amphiboles are hydrous double chain silicates commonly found in igneous and metamorphic rocks. These minerals can incorporate a variety of cations and anions in their structure which can provide clues as to their formation and fluid-rock interactions. The general amphibole composition is $AB_2C_5T_8O_{22}W_2$ and the cations in the B-site defines the subgroup that the amphibole belongs to. For the purposes of this study, which focuses on those amphiboles with substantial Cl contents, Ca-amphiboles are of most interest. In this subgroup the A-site typically contains K and/or Na, the B-site is dominated by Ca for calcium amphiboles but may also contain Fe, Mg, and Na, the C-site contains a combination of Fe^{2+}, Fe^{3+}, Mg, and Al, the T-site mainly contains Si and Al, and the W-site mostly consists of OH^- but also may have Cl^-, O^{2-}, and/or F^- (Hawthorne and Oberti, 2007).

Commonly amphiboles contain OH^- in the W-site but, occasionally the OH^- can be substituted by F^- and/or Cl^-. This can, in part, be attributed to the ionic radii of these molecules. OH^- has an ionic radius of 1.32 Å, while F^- has a similar ionic radius of 1.29 Å (Shannon, 1976). This replacement of OH^- and F^- has been studied by many in the past 100 years (e.g., Bowen and Schairer, 1935; Comeforo and Kohn, 1954; Robert et al., 1989; Pavlovich and Jenkins 2003). Cl^- is a much larger molecule at 1.81 Å making it

harder to squeeze into the W-site and substitute for the OH^- making this a much less common substitution (Shannon, 1976). Recent interest in these Cl-rich amphiboles have

sparked research delving into what crystal chemical controls, brines, and conditions these amphiboles need to accept Cl into their structure.

Chan et al. (2016) and Campanero and Jenkins (2017) looked at different brine compositions during syntheses of ferro-pargasite and hastingsite. It was found that using $FeCl_2$ would yield amphiboles with higher concentrations of Cl about 4x greater than Cl yield when using a NaCl brine (Chan et al., 2016). Crystal chemical controls on Cl acceptance into amphiboles was looked at by Mueller et al., 2017. This study found that higher Fe# in the C-site would increase the chances of Cl in amphiboles. Another study (Jenkins, 2019) looked at K/Na in the A-site and found that K was also correlated with higher Cl acceptance in these amphiboles. Most recently, the pressure and temperature stability of potassium-chloro-hastingsite was investigated by Matteucci (2019) which serves as the experimental basis for deriving the thermochemical properties of potassic-chloro-hastingsite.

In nature Cl is introduced into amphibole by halogen-rich metamorphic/magmatic fluids and may replace some or possibly all the OH in its structure. This can occur in a variety of geological settings: (1) hydrothermal alteration of oceanic crust where halogens are introduced by seawater interacting in the process (Barnes and Cisneros, 2012; Kendrick et al., 2015); (2) the introduction of halogen-rich metasomatic fluids in shear zones (Kusebauch et al., 2015) and in the mantle (Frezzotti et al., 2011); (3) in high grade metamorphic terrains (Léger et al., 1996; Morrison, 1991; Henry and Daigle, 2018), and (4) transportation of ore metals in halogen rich fluids in the formation of economic deposits (Kusebauch et al., 2015).

A thermochemical analysis of amphiboles can provide more details about the halogen fluid composition in these geologic processes. Though a few fluid inclusions can be found in metamorphic rocks it is still difficult to determine fluid composition with just these inclusions. During metamorphism these fluids may come into contact with amphiboles, and this can cause Cl uptake into its W-site. The thermochemical properties of these amphiboles can then be used to predict chloride concentrations of former aqueous fluids (Zhu and Sverjensky, 1991).

This study will focus on determining these properties by synthesizing Cl-rich hastingsite for the purpose of calorimetric measurements of heat capacity, using the thermal stability of hastingsite (Matteucci, 2019) to extract enthalpy and entropy data, and applying these data to metamorphic rocks found in the Black Rock Forest in Cornwall, NY. This area lies within the Hudson Highlands in NY containing a series of metamorphosed gneisses dating back to the Grenvillian Orogeny (~1100 Ma) (Léger et al., 1996). The amphiboles found in these gneisses contain up to ~1.3 apfu Cl. By analyzing amphiboles and the coexisting minerals in this region, the activity of chloride and possibly the composition of the metamorphic fluids that formed these rocks may be determined.

2. Methods

Starting Materials

Materials involved in amphibole syntheses include reagent-grade oxides, carbonates, metallic iron, and "$FeCl_2$". Silicic acid hydrate ($SiO_2 \cdot xH_2O$) was heated overnight in a Deltech furnace at 1100°C to drive off water and form anhydrous SiO_2. Silicon dioxide (SiO_2), aluminum oxide (Al_2O_3), calcium carbonate ($CaCO_3$), and potassium carbonate (K_2CO_3) were weighed and mixed in acetone until dry and heated at 900°C for 15 min to effectively decarbonate the mixture and minimize the loss of potassium. K_2CO_3 was difficult to measure as it was very hygroscopic; to combat this it was heated in the oven at 160°C for 10 min and weighed, then the sample was dispensed, and the empty flask was weighed again. Metallic Fe, iron oxide (Fe_2O_3), and "$FeCl_2$" (a mixture of $FeCl_2$ and $FeCl_2 \cdot xH_2O$) were the main sources of Fe^{2+} and Fe^{3+}. This entire mixture was ground, mixed dry, and heated at 160°C for 15 min just before sealing in a sample capsule for treatment.

Sample Treatment

Capsules made of a $Ag_{50}Pd_{50}$ alloy with a 4 mm diameter and 0.13 mm wall thickness were used in these experiments. This alloy is preferred for these amphibole syntheses for a couple of different reasons. The first reason is that Fe will not get absorbed into this material so easily, a useful characteristic for syntheses of iron-rich

amphibole (Driscall et al., 2005). It is also permeable to H_2 gas which creates a reducing environment that is ideal for amphibole formation (Jenkins, 2019).

Each $Ag_{50}Pd_{50}$ capsule was made from tubing cut about 1.2 cm in length, cleaned with acetone, and annealed at approximately 900°C. One end was then welded together and about 90-100 mg of sample added. Before closing the capsule, it was placed in an oven in air at 160°C for about 15 min, then crimped while still hot. This was done to ensure minimal moisture in the capsule. Lastly, a final weld was made to the crimped end.

Welding was achieved using a carbon-arc welder. Welding a $Ag_{50}Pd_{50}$ alloy with carbon exposes it to oxygen which creates a bubbly, porous, and permeable surface. So, to ensure a smooth weld a lightly moistened tissue was placed over each crimp before welding it. The water in the tissue boils in the heat and masks that oxygen, keeping it from entering the capsule.

Experimental Appartus

Externally heated cold seal vessels were used for the first initial experiments. The vessel itself is made with René 41 (a nickel alloy) with 1.25 in OK and 0.25 in ID, or a 5:1 ratio. Water is the pressure medium and an iron rod (1cm long by 0.4 cm diam.) was placed next to the capsule to reduce the oxygen fugacity inside the vessel. These runs were done at pressures of 2-3 kbars and temperatures of 600 – 650°C for around 2-7 days. After each run the samples were weighed, punctured, dried, and reweighed to account for any weight loss attributed to water.

Internally heated gas vessels were used for most runs. A mixture of H_2 – Ar gas was used to pressurize the vessel. H_2 was pumped in first to the desired pressure to create

a reducing environment. Argon was then introduced to a pre-determined pressure after the H_2 and thermal expansion brought the run up to the desired pressure. Temperature was measured with 2 Inconel-sheathed chromel-alumel thermocouples. Each run was done at 3 – 3.5 kbars and ~700°C. Afterwards, the capsules were weighed, punctured, and soaked in deionized water for ~2 – 3 days before the sample was extracted. This was done to dissolve out any salts that were not part of the synthesized material for the purpose of confirming mass balance with the bulk composition as weighed (see below).

Analytical Equipment and Procedures

Inductively Coupled Plasma Optical Emission (ICP-OES) analysis for Ca, Fe, and K and Ion Chromatography analysis for Cl was done on the salts dissolved out of the capsules. This was done to confirm the composition of the synthetic amphibole by mass balance with the bulk composition and to see how much Cl did not substitute into the amphibole.

Powder X-ray diffraction analysis (XRD) was performed using the Panalytical Xpert PW3040 diffractometer. A small amount of powdered sample was placed on a zero-background single crystal quartz-plate. Operating settings were at 40 kV, 20 mA, and CuKα radiation was used. After all the samples were synthesized and combined (KHAST-1) some of the powder was analyzed over a longer time and heated to 600° C to ensure its stability for differential scanning calorimetry (DSC) measurements. This sample was scanned from 5-100°, with a step size of 0.05° and counting time of 1 second per step.

Rietveld refinement was performed using GSAS II (Toby and Von Dreele, 2013). Crystal structure data used for initiating the refinements came from the American

Mineralogist Crystal Structure Database. Three minerals were used for the refinements: hastingsite (Makino and Tomita, 1989), fayalite (Smith and Hazen, 1973) and magnetite (Weschler et al., 1984). The hastingsite structure was refined to more accurately reflect the hastingsite being refined. Cl was added and Na was removed from the structure and replaced by K.

Refinements started by fitting a Chebyshev equation to the background of the patterns. From there each mineral (amphibole, fayalite, magnetite) was included in the refinement process one parameter at a time. This process ended when chi^2 reached a minimum.

Electron microprobe analysis was performed on the JEOL 8900 Superprobe. Powdered samples were mounted in epoxy and thin sections from the Black Rock Forest Consortium were both polished with diamond grit down to 0.5 μm. The operating conditions of the microprobe were at 15 kV and 10 nA and matrix corrections used ZAF terms. Wollastonite was used as the standard for Ca, orthoclase for K, albite for Na, hematite for Fe, corundum for Al, quartz for Si, TiO_2 for Ti, fluor-apatite for F, chromite for Cr, spessartine for Mn, and $PdCl_2$ for Cl. Initially weight percentages of the minerals were recast using 24 oxygens at the time of analysis. They were then recast based on the minerals found. Amphiboles were recast with the sum of O + Cl + OH = 24, K-spar and plagioclase with 8 oxygens, magnetite with 4 oxygens, pyroxene with 6 oxygens, chlorite with 14 oxygens, serpentine with 7 oxygens, and garnet with 12 oxygens.

Fourier Transform Infrared Spectroscopy was performed on a Bruker Tensor 27 at Binghamton University. Samples were embedded in ½-inch diameter KBr pellets at the ratio of 3 to 6 mg of sample to 200 mg of KBr. Scans were made using 64 repetitions at a

resolution of 2 cm^{-1} in a nitrogen atmosphere. This analysis was used to determine how much if any OH was present in the samples.

Differential Scanning Calorimetry was performed on the synthetic amphibole to measure its heat capacity and, eventually, to derive a heat capacity expression for end-member potassic-chloro-hastingsite. These experiments were performed by Sitaram Panta and Prof. Eric Cotts in the Physics department of Binghamton University using a Perkin Elmer DSC-7 calorimeter. Around 50 mg of sample was sent to the department to analyze. This calorimeter uses small sample pans, one of which would be filled with the sample (KHAST-1) and the other with a standard (corundum). These were heated in intervals from 30°C -534°C. For example, heating from 30°C - 135°C went as follows: 1) sample heated from 30°C to 60°C at a rate of 60°C/min, 2) temperature was isothermally held at 60°C for 4 minutes, 3) pans heated from 60°C - 135°C at a rate of 20°C/min, and 4) temperature isothermally held at 135°C for 6 min. This process was done at intervals up to 534°C.

Field Methods

Rocks from the Black Rock Forest Consortium located in Cornwall, NY were collected and analyzed for Cl-rich amphiboles and their coexisting minerals. Maps in the paper by Léger et al. (1996), NYS geological survey maps, and trail maps provided by the consortium were used to target specific locations of collection in the forest. Rock hammers were used to collect fresh samples that were bagged and tagged and brought back to the university. GPS coordinates were also recorded to provide the exact locations that these samples were collected (Figure 1). Back at the university 16 samples were selected to represent the different locations of collection and made into thin sections. There were 2 thin sections made from each sample, the first was ground down to the standard thickness of ~30 μm to study under the microscope to determine the mineral assemblage in the rocks. The second thin section was much thicker and was analyzed with the microprobe.

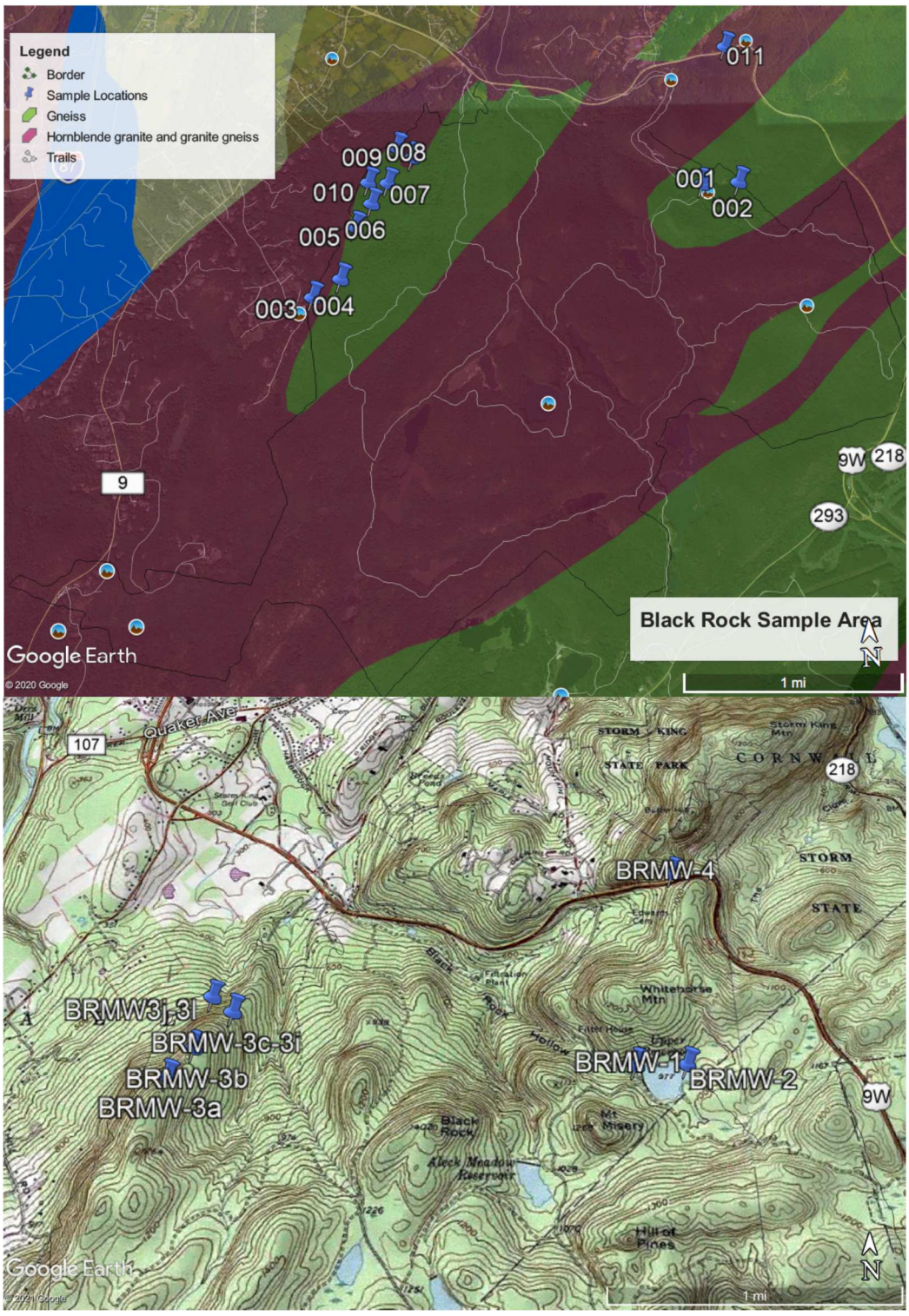


Figure 1: (a) Locations of samples collected in the Black Rock Forest. (Google Earth and NY State Geologic Maps used, trail data from the Black Rock Forest Consortium website). (b) Topographic view of the Black Rock Forest and sample locations.

3. Results

Characterization of synthetic amphibole

The bulk composition for these experiments were based on the ideal K-Cl hastingsite composition $KCa_2(Fe_4Fe^{3+})(Al_2Si_6)O_{22}Cl_2$. Amphiboles were synthesized at 1.98-3.45 kbars and 650-700°C. Each run yielded mostly amphibole with some fayalite and magnetite; conditions and products of these experiments can be seen in Table 1.

Unfortunately, syntheses rarely yield the pure endmember or even complete amphibole yields and instead other minerals may form and some of the material may not be incorporated into the desired product. It was also noted that coexisting Fe-rich salts were generally not well crystallized and their presence was not readily detected by X-ray diffraction. To account for this, a mass-balance determination was done between the synthesis products and the bulk composition of the starting material using a combined wet-chemical and X-ray diffraction analysis as follows. First, a small cut was made in each capsule after it was retrieved from the pressure vessel and soaked overnight to draw out any unincorporated salts. They were then diluted in 100 mL of deionized water and analyzed by ICP-OES and ion chromatography. Rietveld refinement was then done on the synthesis products to determine the proportions of crystalline phases present. For KHAST-1a, -1b, and -1d a small amount of fayalite was found, while for KHAST-1f a small amount of magnetite was also found coexisting with amphibole. The proportions of amphibole, fayalite, and magnetite in each sample was determined during this refinement and are indicated in Table 1.

Microprobe analyses were next obtained for the amphibole in each sample (Table 2) and each element was converted to a total mass. This was done by taking the mass of the synthesis products that were not dissolved in solution, the percentage of that sample that was amphibole (determined from Rietveld refinement), and the total mass of each element in each solid phase produced in the syntheses. Fayalite was present and the total mass of Fe, Si, and O in fayalite was determined similar to amphibole. The water into which the salts were dissolved was analyzed for K, Ca, Fe, and Cl. Combining the masses of each element in amphibole, fayalite (KHAST-1c, -1e), and aqueous solution, these total masses were compared to the theoretical masses of each element in the starting mixture (Table 3). The Cl was generally found to be much higher than would be expected. The origin is unknown but likely came from some contamination in the deionized water used to soak the capsules. Overall, each sample shows good agreement between the observed and expected mass for each element analyzed (Figure 2).

Table 1: Conditions and products of the amphibole syntheses comprising KHAST-1.

Sample	P (kbars)	T (°C)	$\Delta \log fO_2$**	Products
KHAST-1a *	1.98	658	NiNiO***	Hastingsite, Fayalite
KHAST-1b	2.90	696.8	0.098	Hastingsite (96.5%), Fayalite (3.5%)
KHAST-1c	3.35	700.5	0.109	Hastingsite (98%)
KHAST-1d	3.45	699	0.03	Hastingsite (97%), Fayalite (3%)
KHAST-1e	3.45	699	0.03	Hastingsite (98%)
KHAST 1f *	2.4	599	NiNiO***	Hastingsite, Magnetite

* Indicates runs with Cold Seal Vessels instead of Gas Vessel

** ΔfO_2 relative to NiNiO

*** Approximate oxygen fugacity

Table 2 : Microprobe analyses of individual K-Cl-hastingsite synthesis samples. Uncertainty (1σ) in last digit given in parentheses.

	KHAST-1b	KHAST-1c	KHAST-1d	KHAST-1e	Average KHAST-1-FM
n	15	10	10	9	44
SiO2	38.00 (26)	37.46 (14)	36.16 (17)	36.54 (36)	37.04 (49)
Al2O3	9.90 (18)	10.10 (9)	10.38 (6)	9.41 (8)	9.95 (22)
Fe2O3*	6.33 (4)	6.61 (2)	6.58 (1)	6.30 (5)	6.45 (7)
FeO*	26.19 (14)	27.10 (10)	26.97 (5)	25.81 (22)	26.52 (28)
CaO	10.60 (10)	10.63 (4)	10.47 (3)	10.12 (11)	10.46 (16)
K2O	3.37 (3)	3.55 (5)	3.57 (3)	3.36 (3)	3.46 (7)
Cl	3.79 (3)	3.84 (2)	4.10 (2)	4.16 (6)	3.97 (7)
Total	98.55 (45)	99.2 (20)	98.64 (20)	96.06 (77)	98.22 (94)
cations**					
^{T}Si	6.49 (3)	6.35 (2)	6.22 (2)	6.47 (1)	6.38 (4)
^{T}Al	1.51 (3)	1.65 (2)	17.8 (2)	1.53 (1)	1.62 (4)
Sum T	8.00	8.00	8.00	8.00	8.00
^{C}Al	0.48 (2)	0.36 (1)	0.33 (1)	0.45 (1)	0.40 (3)
^{C}Fe^{3+}	0.82	0.85	0.85	0.84	0.84 (1)
^{C}Fe^{2+}	3.70 (2)	3.78 (1)	3.82 (1)	3.72 (1)	3.75 (2)
Sum C	5.00	4.99	5.00	5.00	5.00
^{B}Fe^{2+}	0.06 (1)	0.07 (1)	0.07	0.09 (1)	0.07 (2)
^{B}Ca	1.92 (1)	1.93 (1)	1.93	1.91 (1)	1.92 (2)
Sum B	1.99	2.00	2.00	2.00	2.00
^{A}K	0.73	0.77 (1)	0.78 (1)	0.76 (1)	0.76 (1)
^{A}Ca	0.01	0.00	0.00	0.01	0.01
Total	15.73 (1)	15.76 (1)	15.78 (1)	15.77	15.76 (2)
Anions					
Cl	1.10 (1)	1.10 (1)	1.20 (1)	1.2 (1)	1.16 (2)
OH	0.38 (3)	0.60 (2)	0.61 (2)	0.2 (1)	0.45 (5)

* calculated from microprobe analyses of total FeO assuming the atomic ratio of $Fe^{3+}/(Fe^{2+} + Fe^{3+}) = 0.18$ (e.g., Mueller et al., 2017).

** Calculated on the basis of O+Cl+OH = 24.0.

Table 3: Mass balance assessment for amphibole synthesis experiments

	KHAST-1b			KHAST-1c		
	Observed Mass		Calculated Mass	Observed Mass		Calculated Mass
	Amph + Soln Total	Std Dev	Ideal Amph	Amph + Fay + Soln Total	Std Dev	Ideal Amph
Si	17.0	0.7	16.7	15.9	0.5	14.6
Al_{Total}	5.0	0.9	5.3	4.1	0.6	4.7
$Fe^{2+}{}_{Total}$+Fe^{3+}	25.5	1.1	27.6	25.8	0.7	24.3
Ca_{Total}	7.8	0.4	7.9	7.2	0.2	7.0
K	3.1	0.2	3.9	3.0	0.3	3.4
Cl*	7.8	0.2	7.0	20.7	0.2	6.2
OH	0.6	0.5	0.0	0.9	0.4	0.0
O	33.5	0.0	34.8	32.0	0.0	30.6
Total	76.5	4.0	103.1	98.8	2.9	90.6
	KHAST-1d			KHAST-1e		
	Observed Mass		Calculated Mass	Observed Mass		Calculated Mass
	Amph + Soln Total	Std Dev	Amph ideal	Amph + Fay + Soln Total	Std Dev	Ideal Amph
Si	14.0	0.4	15.3	16.2	0.3	14.5
Al_{Total}	4.6	0.6	4.9	4.6	0.4	4.7
$Fe^{2+}{}_{Total}$+Fe^{3+}	22.6	0.4	25.4	25.0	0.5	24.1
Ca_{Total}	6.9	0.1	7.3	7.2	0.3	7.3
K	2.9	0.2	3.5	3.0	0.2	3.5
Cl*	13.4	0.3	6.4	15.9	0.4	6.1
OH	0.2	0.2	0.0	0.3	0.2	0.0
O	29.0	0.0	32.0	32.2	0.0	30.3
Total	93.6	2.4	94.7	104.4	2.3	90.0

* Cl for sample KHAST-1b fell within reasonable values. The Cl for the other 3 samples were not within reasonable values possibly due to contamination.

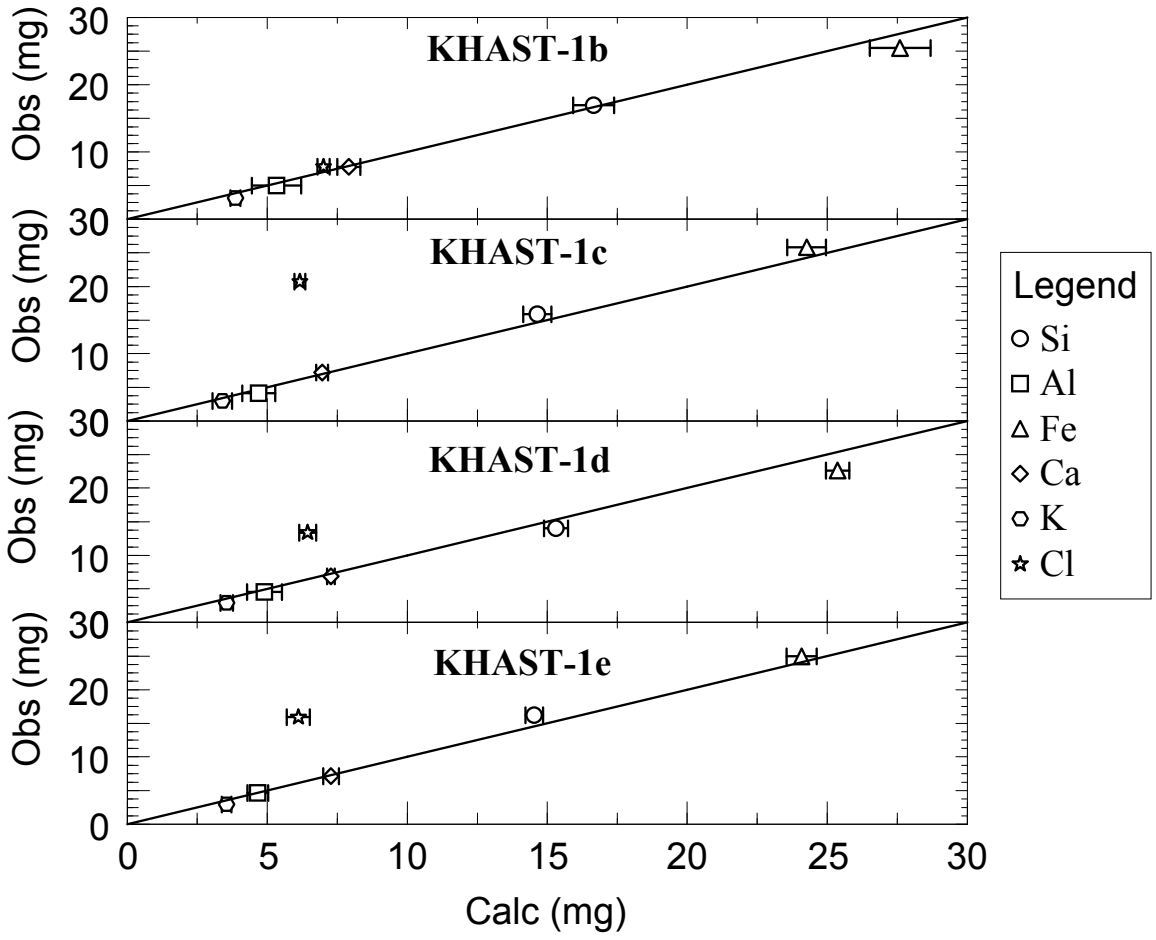


Figure 2: Mass-balance assessment of the amphibole synthesis products from this study. Comparison of observed (Obs) and theoretical (Calc) masses of individual elements as listed in Table 2. (a) Sample KHAST-1b. (b) KHAST-1c. (c) KHAST-1d. (d) KHAST-1e. The diagonal line represents the expected 1:1 correlation.

FTIR Analysis

Although the amphibole made in this study was synthesized under dry conditions to be close to the K-Cl hastingsite endmember, some OH can make its way in during the synthesis. Fourier Transform Infrared Spectroscopy was performed on KHAST-1-FM and a sample of synthetic pargasite (PARG 11-7, Sharma and Jenkins, 1999) to estimate the H_2O content of the former using the theoretical H_2O content of the latter. Figure 3 shows specifically the OH stretching region of the pargasite (black line) and KHAST-1-FM (red line). Each curve was then fitted with two bands in Figure 4 and the peak area integrated in Highscore to get the approximate amount of OH in these samples. The total fitted area for KHAST-1-FM was 2198 and for PARG 11-7 it was 5758 ($a \cdot cm^{-1}$). Finally, by dividing the peak area of KHAST-1-FM by the peak area of pargasite and multiplying by the wt% of H_2O in pargasite (2.02 wt%) the water content in the amphibole comes to 0.77 wt %.

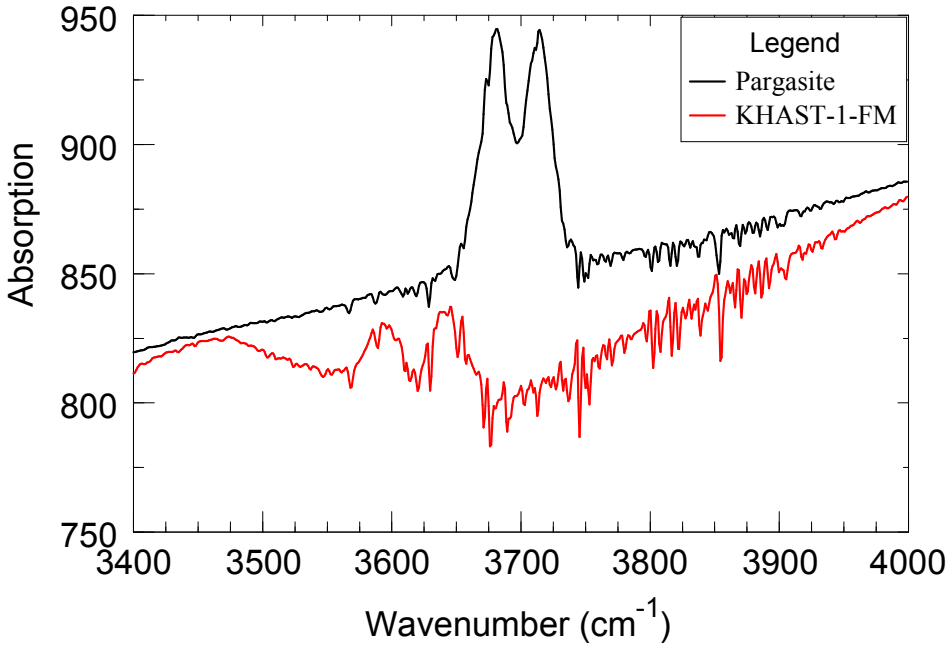


Figure 3: FTIR analysis of synthetic pargasite (black curve) and KHAST-1-FM (red curve) in the OH-stretching range.

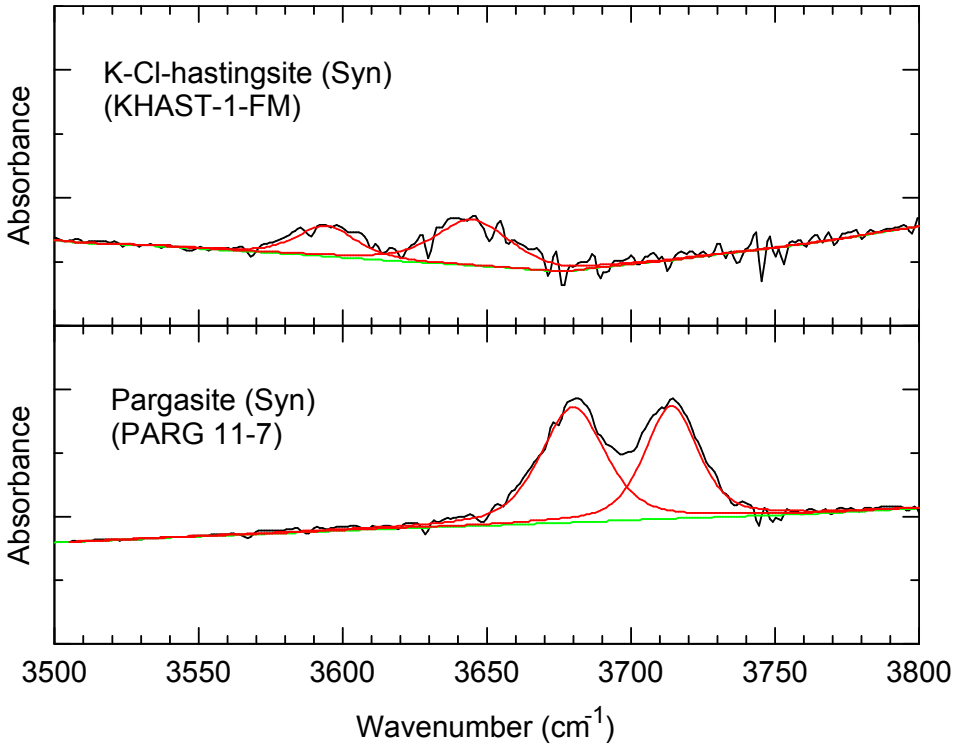


Figure 4: OH stretching region of KHAST-1-FM (top) and synthetic pargasite (bottom). to determine approximate wt% of H_2O in KHAST-1-FM. Original data (black), fitted peaks (red), and background fit (green),

Heat capacity determination

Once sufficient synthetic amphibole was made the next step was to determine its heat capacity; the heat capacity of K-Cl hastingsite, or indeed of most Fe-rich amphiboles, is simply not known. Heat capacity was determined using two different methods. The first was a summation method which basically involves summing the heat capacities from different minerals to come up with the ideal amphibole formula and an estimate for the ideal amphibole Cp.

The second involved direct measurement. The individual amphibole syntheses (Table 1) were combined into one sample (KHAST-1-FM) to (a) analyze how temperature would affect the stability of the amphibole, and (b) to have calorimetry measurements performed on it to determine its heat capacity. High temperature XRD scans were done at temperatures up to 600°C in 100°C increments, with the last scan performed after the sample was kept at 600°C for 1 hour. The sample was mounted on an Al plate which gives the scan 2 extra peaks from the (111) at around 38.5°2Θ and (200) at around 44.7°2Θ. Also, greater thermal expansion of the Al plate relative to hastingsite causes noticeable Al peak shifts (to lower angles) going from 25°C to 600°C. As the sample was heated the scans stayed consistent with each other indicating no physical change to the amphibole as temperature changed (Figure 5). This ensures that the amphibole would remain stable during DSC measurements which ranged from 25°C to 550°C.

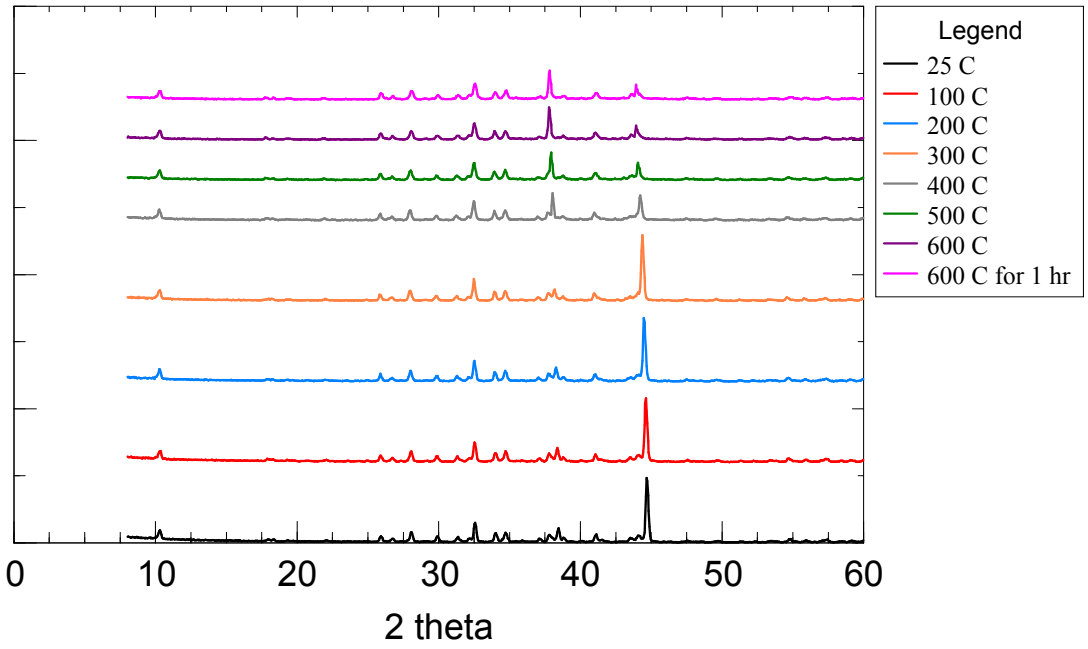


Figure 5: Thermal scans of synthetic K-Cl-hastingsite (KHAST-1-FM) made at increasing temperatures from 25°C (bottom) to 600°C (top) . The upper-most pattern is from the amphibole sitting at 600°C for 1 hour.

The heat capacity for both synthetic KHAST-1-FM and natural tremolite from Barrie Township, Ontario, Canada (Jenkins, 1987) was measured using differential scanning calorimetry performed by Sitaram Panta (Physics Department, Binghamton University). The precision of these measurements is ~4% and for some values closer to 5%. Tremolite is very well-studied and was used to demonstrate consistency of the tremolite Cp values with literature (Figure 6).

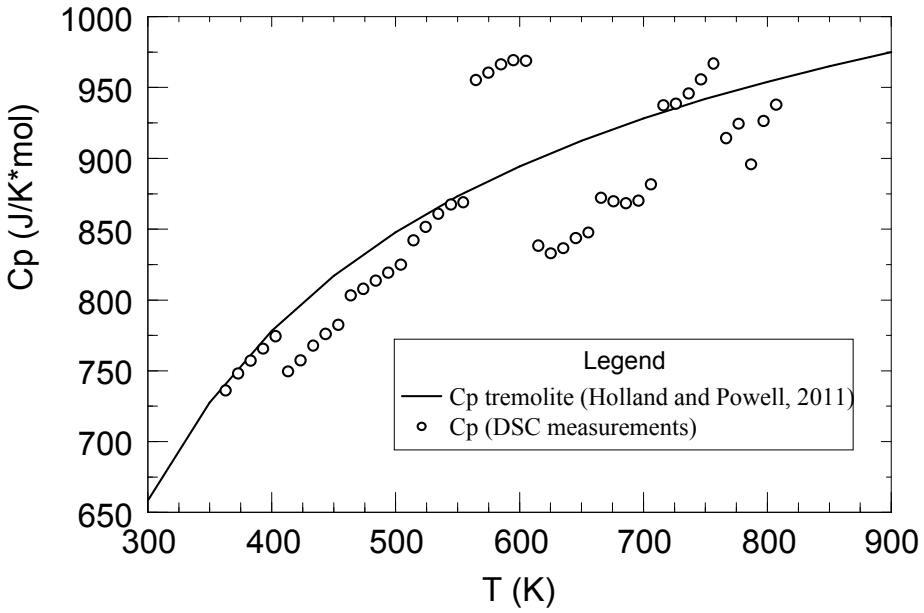


Figure 6: Cp Tremolite from DSC measurements compared to Holland and Powell, 2011 Cp data.

Both tremolite and KHAST-1-FM were measured with DSC at intervals from ~300-800K (Figure 7). Over most temperature intervals there was an offset between the two sets of data, but the offsets were at least consistent between tremolite and hastingsite. At select intervals from ~300-400, 450-600, and ~700K both tremolite and hastingsite were offset in a similar manner. In the end, only those narrow temperature intervals where tremolite was in close agreement with the published data from Holland and Powell (2011) were used to constrain the Cp expression for KHAST-1-FM, as shown in Figure 8.

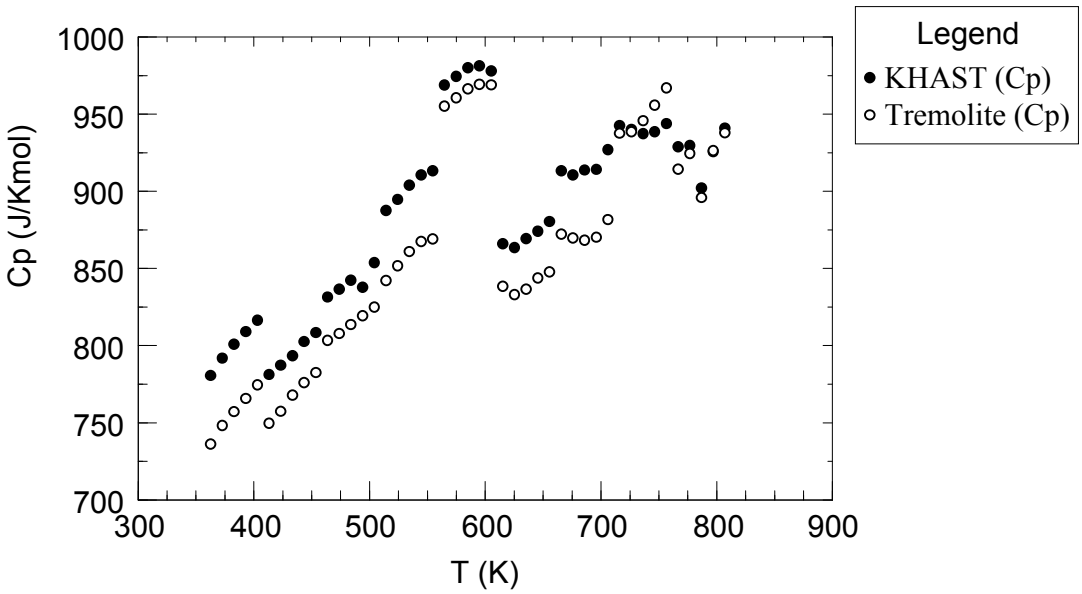


Figure 7: Raw Cp (J/K·mol) data for both KHAST-1 and Tremolite

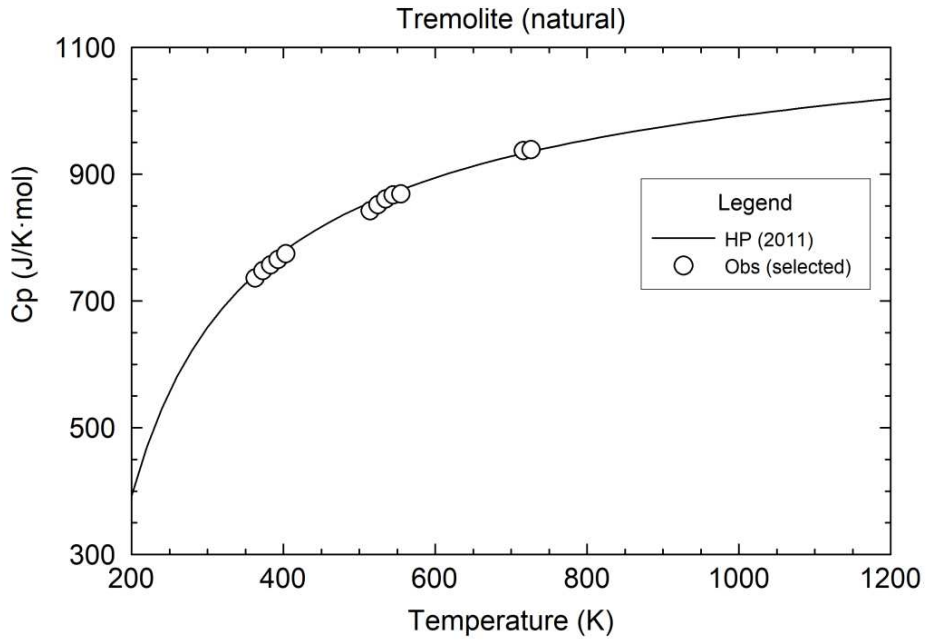


Figure 8. Selected DSC data for natural tremolite matching the published Cp expression of Holland and Powell (2011, HP 2011)

Given the limited range of data accepted to constrain the KHAST-1-FM Cp expression, the Cp expression was modeled after the ferroactinolite Cp expression of Holland and Powell (2011) and the initial constant, or *a*-term, was adjusted to fit the ferroactinolite Cp curve to the hastingsite Cp data (Figure 9). The Cp expression adopted in this study for KCH is Cp (kJ/K·mol) = $1.290 + 2.9992\text{x}10^{-5}\text{T} - 8447.5/\text{T}^2 - 8.947/\text{T}^{1/2}$, where T is temperature in Kelvins. The resultant Cp expression gives the curve (solid black) in Figure 9 compared to the measured data (circles).

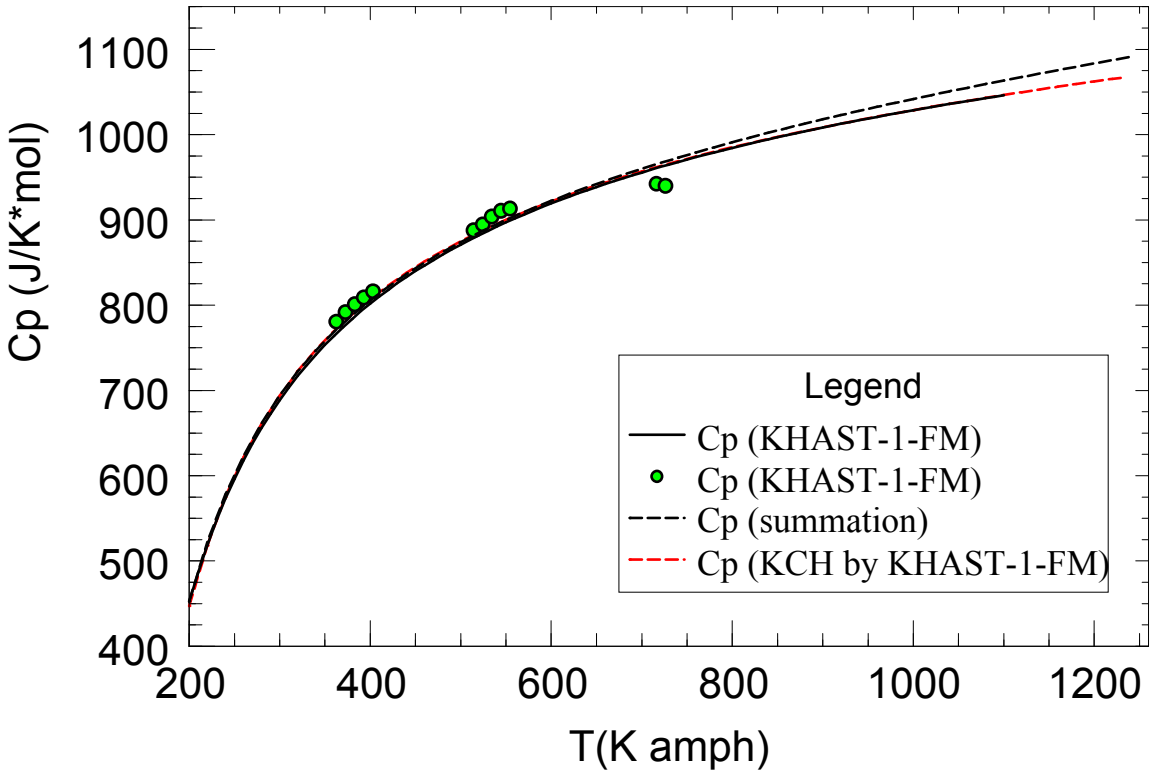


Figure 9: Synthetic amphibole (KHAST-1-FM) Cp data from this study (circles) modeled after the ferroactinolite Cp curve from Holland and Powell (2011), giving the Cp curve used in this study (solid black). For comparison, the Cp curve for ideal K-Cl-hastingsite (KCH), extracted from the Cp expression for the synthetic KHAST-1-FM amphibole as discussed in the text, is shown by the red dashed curve. The black dashed curve is the Cp estimated by summing mineral components, as discussed in the text.

For comparison, it is possible to estimate the Cp expression for ideal K-Cl-hastingsite (KCH) by summing the appropriate mineral components. This was done using the reaction:

KCH = Pargasite – 4/5 Tremolite + 4/5 Ferro-actinolite + $CaCl_2$ – $Ca(OH)_2$ + Leucite – 2 Jadeite + Acmite

The heat capacity data for each phase came from Holland and Powell (2011) and Robie and Hemmingway (1995).This Cp summation is shown by the black dashed line on Figure 9 which follows closely to the measured Cp of KHAST-1-FM up to around 800 K where it starts to deviate.

Finally, we can correct the Cp expression for KHAST-1-FM to account for small deviations from ideal K-Cl-hastingsite (= KCH) using the averaged analysis from Table 2. Ideal K-Cl-hastingsite can be related to KHAST-1-FM (= Amph) by the following corrections:

1.0 KCH = 1.25 Amph + 0.25 $FeCl_2$ – 0.3125 Fay – 0.9375 Qtz – 0.375 Hed – 0.5 Diasp

where Fay is fayalite, Qtz is quartz, Hed is hedenbergite, and Diasp is diaspore. The Cp expressions for all phases were taken from Holland and Powell (2011) except for $FeCl_2$ (lawrencite) which was taken from Robie and Hemingway (1995). The resultant extracted Cp expression for ideal KCH is shown as the red-dashed curve in Figure 9 which is virtually identical to the Cp curve for KHAST-1-FM based on ferro-actinolite. The deviations from the summation Cp curve (black dashed) are also very trivial.

Enthalpy and Entropy

Enthalpy and entropy were calculated using the Gibb's Free Energy equation:

$$\Delta G=0= \Delta H°\text{-}T\Delta S°+ \int_{T°}^{T} \Delta Cp\ dT \text{ -}T \int_{T°}^{T} \Delta Cp/_{T}\ dT+ P*\Delta V^{solids} + RTlnKa+RTlnfO_2 . \quad (1)$$

$P\Delta V^{solids}$ is an integration of $\int_{Po}^{P} \Delta V^{solids} dP$ because we are adapting values for thermal expansion (α), and bulk modulus terms (κ, κ', κ'') for the amphibole (Table 6).

If heat capacity, pressure, volume, oxygen fugacity, and activities of components in any solid (e.g., amphibole, pyroxenes) is known then these can be condensed down to a known value G'.

$$G' = \int_{T°}^{T} \Delta Cp\ dT\ - T \int_{T°}^{T} \Delta Cp/_{T}\ dT + P*\Delta V^{solids} +\ RTlnKa + RTlnfO2$$

$$= -\ \Delta H° + T\Delta S° \quad (2)$$

The heat capacity was determined above to be Cp (kJ/K·mol) = $1.29 + 2.9992x10^{-5}T - 8447.5/T^2 - 8.947/T^{1/2}$. The volume was determined using the unit cell parameters from Rietveld refinements done on KHAST-1-FM and other K-Cl-hastingsite-rich amphibole that were synthesized by Jared Matteucci (M.S. Thesis, 2019). These parameters were for amphiboles containing up to ~1.2 apfu Cl and are plotted in Figure 10. A straight-line fit to all of this data was extrapolated to 2.0 apfu Cl to determine the volume for ideal K-Cl hastingsite to be 960.6 A^3 (Figure 10).

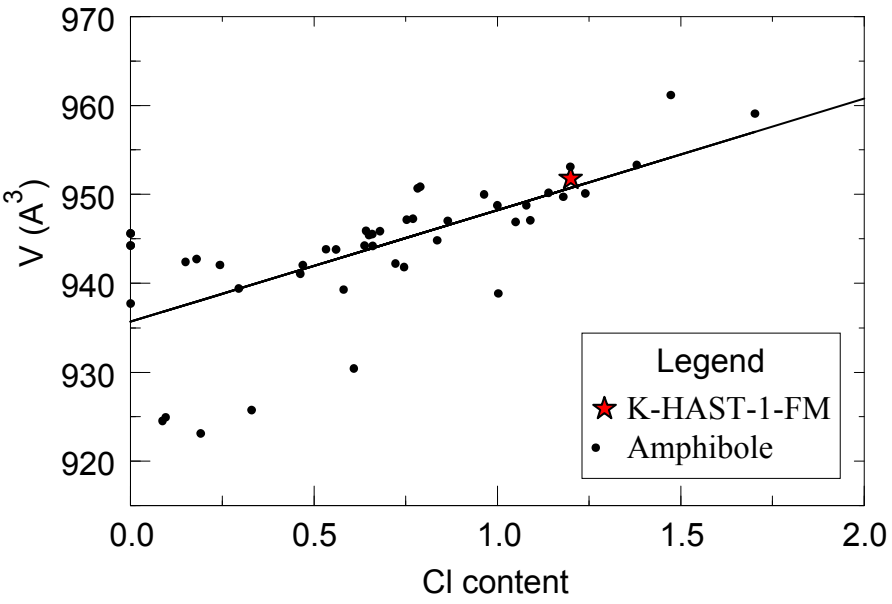


Figure 10: Volumes of synthetic K-Cl hastingsitic amphiboles with Cl amounts of 0 – 1.7 apfu from this study (star) and Matteucci, 2019 (circles)

The equilibrium constant (K_a) needs to be determined to calculate G'. This starts with a balanced reaction which was derived using the known breakdown products of K- and Cl-rich hastingsitic amphibole from Matteucci (2019) (Amph, Figure 11). This reaction, expressed for the end-member compositions, was determined to be:

$$4\ KCH = 4\ An + 1\ Qtz + 4\ Hed + 7\ Fay + 2\ FeCl_2 + 4\ Syl + 1\ O_2. \quad (3)$$

where KCH is ideal K-Cl-hastingsite, An is anorthite, Qtz is quartz, Hed is hedenbergite, Fay is fayalite, and Syl is sylvite. There are only 2 minerals that would be considered in the K_a expression that are not pure end-member phases, which would be KCH and Hed. This makes K_a:

$$K_a = \frac{(a_{Hed}^4)}{a_{KCH}^4} \quad (4)$$

The program AX (Holland, 2019), a program which uses the mineral compositions expressed in wt% of the oxides or cations to calculate the activities of mineral endmember components consistent with the Holland and Powell (2011) database, was used to calculate hedenbergite activities in the clinopyroxene. This activity was calculated to be around 0.73-0.75. Amphibole components in K-Cl-hastingsite can not be calculated with the AX program, so it was calculated as an ideal activity using the mole fractions of each element:

$$a_{ideal}\ KCH = 8\ (X_K^A)(X_{Ca}^{M4})^2(X_{Fe}^{M13})^3\left(X_{Fe^{3+}}^{M2}\right)(X_{Al}^{M2})(X_{Al}^{T1})^{0.5}(X_{Si}^{T1})^{0.5}(X_{Cl}^{w})^{\frac{2}{3}} \quad (5)$$

This expression is modeled after ideal-activity expressions used in the Holland and Powell (2011) data base, as discussed in Diener et al. (2007) and Chan et al. (2016) and further discussed in the Discussion section. The ideal activity for the K-Cl hastingsite in the amphibole participating in the breakdown reaction in Figure 11 was calculated to be 0.169.

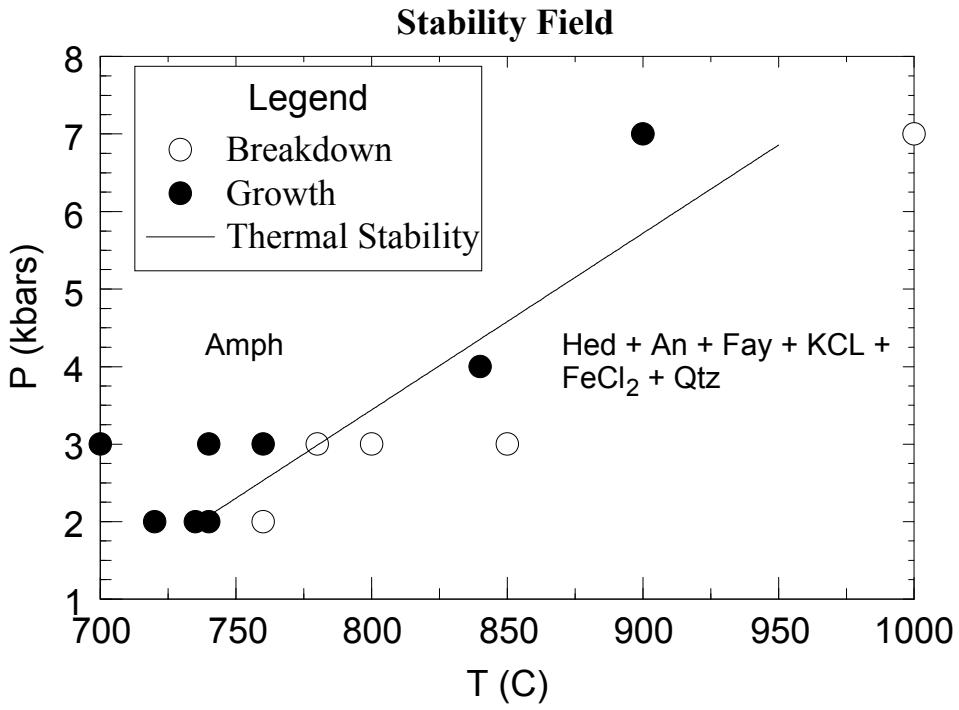


Figure 11: Thermal stability field of synthetic K-Cl hastingsitic amphibole (Amph).

Table 4. Hedenbergite produced in reaction (3)	
Wt %	
SiO2	45.4
Al2O3	6.5
FeO	29.8
CaO	18.3
K2O	0
Cl	0
Fe2O3	0
Sum	100
Cations	
Si	1.9
Al	0.3
Fe3+	0
Fe2+	1.0
Ca	0.8
K	0
Cl	0
Total	4.0
Activity	
Hedenbergite	0.75
Ca Tschermakite	0.31

The last piece of information needed to come up with the enthalpy and entropy of K-Cl hastingsite is the oxygen fugacity (fO_2). The experiments were conducted near the NNO buffer (Table 1). The oxygen fugacity was calculated using oxygen fugacity over a range of pressures and temperatures (Figure 12) using the expression for the NNO buffer given in Frost (1991).

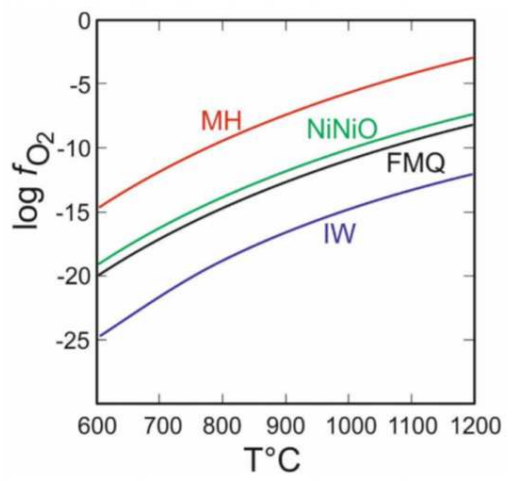


Figure 12: Oxygen fugacity (Frost, 1991)

Once the heat capacity, volume, activities of the amphibole and breakdown product pyroxene, and fO_2 have been determined, G' can be calculated. Each G' was calculated over four temperature and pressure ranges (Table 5). These values were then plotted, and a straight line fit to them (Figure 13). The slope for this fit is 0.407 kJ/K·mol ($\Delta S_{reaction}$) and the y-intercept is -675.11 kJ/mol ($\Delta H_{reaction}$). These values include values for both the breakdown products and amphibole so they are further adjusted to reflect just the amphibole's enthalpy and entropy. This is done by taking the sum of all the products and subtracting from these the $\Delta H°_{reaction}$ and $\Delta S°_{reaction}$, respectively.

$$\Delta H° \text{ (KCH)} = (H_{Qtz} + H_{O2} + 2H_{FeCl2} + 4H_{syl} + 7H_{Fay} + 4H_{Hed} + 4H_{An}) - \Delta H°_{reaction} \quad (6)$$

$$S° \text{ (KCH)} = (S_{Qtz} + S_{O2} + 2S_{FeCl2} + 4S_{syl} + 7S_{Fay} + 4S_{Hed} + 4S_{An}) - \Delta S°_{reaction} \quad (7)$$

Once this has been done the enthalpy of ideal K-Cl-hastingsite (KCH) is found to be -10,664.5 kJ/mol and entropy to be 741.23 J/K·mol. The thermochemical data determined in this study for KCH are summarized in Table 6.

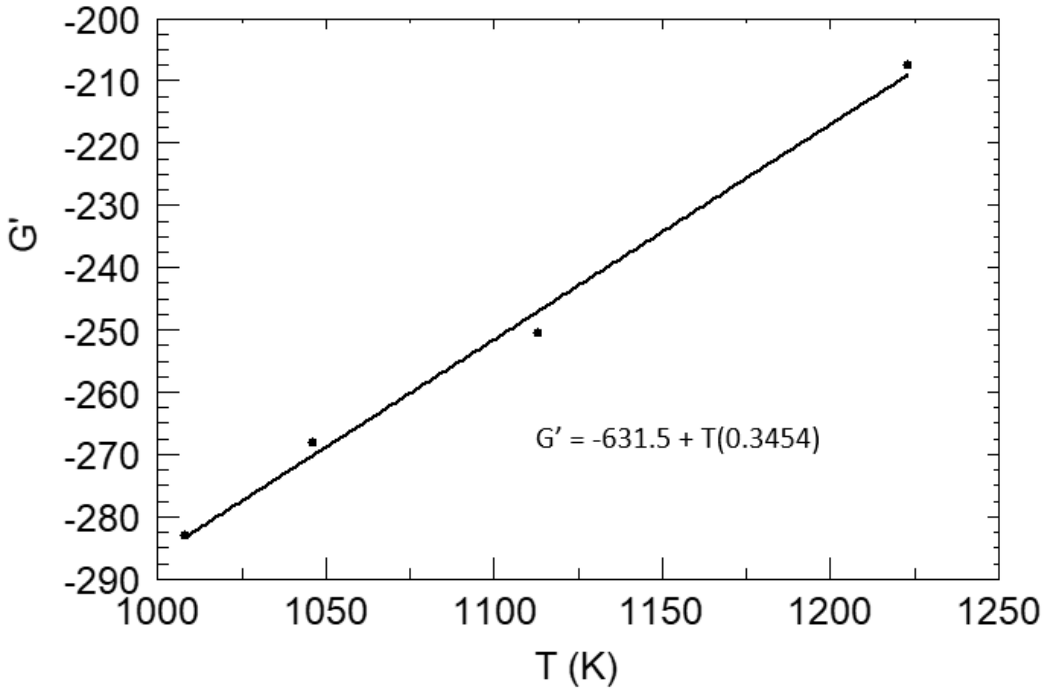


Figure 13. Graph of G' (kJ) values plotted against temperature and fit with a straight line to determine enthalpy and entropy.

Table 5: Reaction-reversal data used for calculating G' at P and T				
P (kbar)	2	3	4	7
T (°C)	735	773	840	950
T (K)	1008	1046	1113	1223
a_{Hed}	0.75	0.75	0.74	0.73
a_{KCH}	0.17	0.17	0.17	0.17
K	392.06	392.06	392.06	392.06
Log(fO2)	-15.28	-14.34	-12.87	-10.76
G' (kJ)	-283.12	-268.09	-250.54	-207.62

Table 6:Thermochemical data of K-Cl hastingsite derived and adopted in this study		
ΔH_f (kJ/mol)		-10653.57
S° (J/K·mol)		756.62
V (A^3)		960.60
V (cm^3/mol)		289.29
Cp (kJ/K·mol)*	a	1.290
	b	1.9992 x 10^{-5}
	c	-8447.5
	d	-8.947
α (K^{-1})**		2.80 x 10^{-5}
κ (kbar)		912.00
κ '		4.09
κ '' ($kbar^{-1}$)		-0.0045

*Coefficients for the expression $Cp = a + bT + c/T^2 + d/T^{1/2}$

** Thermal expansion (α) and bulk modulus values (κ, κ', and κ'') for pargasite from Holland and Powell (2011) were adopted here.

4. Discussion

Stability curve for ideal KCH

Now that the thermochemical data for ideal KCH have been derived the stability boundary for ideal KCH can be calculated. This can be done by setting Ka to 1 for the ideal end-member reaction (3). When compared to the experimental stability curve, the ideal stability boundary for KCH is shifted to lower temperatures (Figure 14). The shifted boundary can be attributed to solid solution in amphibole.

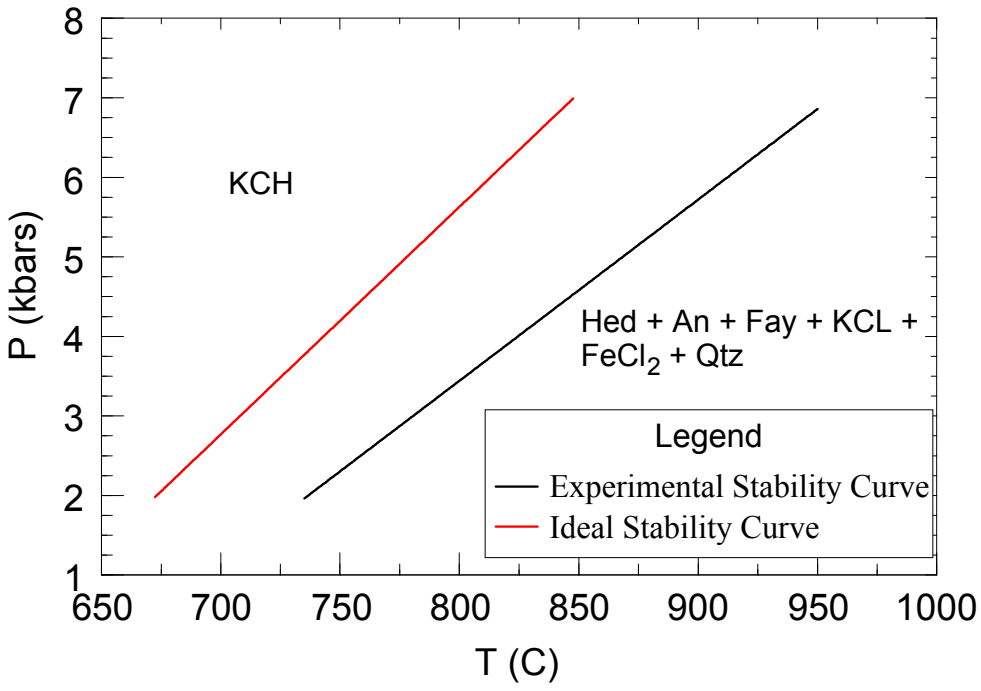


Figure 14: Thermal Stability of K-Cl hastingsite. Experimental thermal stability (black line) as shown in Figure 11 compared to the ideal thermal stability (red line) derived using the new thermochemical data.

Black Rock Forest: sample descriptions

Rock samples were collected from the Black Rock Forest in Cornwall, NY, to apply the newly derived data on potassic-chloro-hastingsite (KCH) to a real-world situation. These are metamorphosed gneisses formed during the Grenvillian orogeny around 1100 Ma at peak metamorphic conditions estimated at 750-800°C and depths of 25-30 km (8-10 kbar) (Léger et al., 1996; Isachsen et al. 2000, p. 48). The rocks in this location were found previously by Léger et al. (1996) to contain amphiboles rich in Cl (~4.6-5.1 wt %). Other major minerals found in these rocks were K-spar, plagioclase, orthopyroxene, clinopyroxene and quartz. Other minor minerals found in these rocks include ilmenite, magnetite, apatite, and sulfides (Léger et al, 1996). The study by Léger et al (1996) includes microprobe analyses of the biotite and amphibole in this region; however, compositions of the other phases, which are needed for calculating the Cl content of the ambient fluid, were not analyzed. The major minerals were analyzed in the samples collected from the Black Rock Forest to determine a balanced reaction expressing the exchange of Cl between a Cl-bearing fluid and the amphibole.

Various samples from 4 different locations were collected from the Black Rock Forest (Figure 1). Three to four samples were selected from each location to be made into thin sections to analyze under the microscope and in the electron microprobe. Minerals observed in these samples are listed in Table 7. The mineral assemblage of these gneisses includes amphibole + quartz + clinopyroxene + orthopyroxene + plagioclase +/- K-spar (microcline and/or orthoclase). Mineral compositions and their normalized formulae (described below) are reported in Tables 7-12.

Table 7: Minerals found in each rock sample indicated by x.

	Rock Sample ID															
Minerals	1b	1m	1v	2I	2r	2t	2v	3a	3e	3k	3r	4a	4c	4e	4h	4f
Amphibole	x	x	x	x	x	x	x	x	x	x	x	x	x	x	x	x
Kspar	x	x	x					x	x	x	x	x	x	x	x	x
Qtz	x	x	x	x	x		x	x	x	x		x		x		
Cpx	x	x	x	x	x	x	x	x			x	x		x	x	
Opx		x	x	x	x	x	x			x	x			x		
Mt	x				x		x		x						x	x
Plag	x	x	x	x	x	x	x	x	x	x	x	x	x	x	x	x
Ilmenite	x	x	x	x	x	x	x	x	x			x	x	x	x	x
Apatite	x	x	x	x	x	x	x	x	x			x	x	x		x
Sulfides	x															

The K-feldspar analyses were normalized to 8 O (Table 8). Of the four locations sampled, only location 2 contained no visible K-spar (optically or under the microprobe). The previous study by Léger et al. (1996) also collected some samples from this location that did not contain K-feldspar. Myrmekitic texture between K-spar and plagioclase can be seen in a few of the samples. K-feldspar also showed alteration in samples from location 4. The ratio of K/(K+Na+Ca) lies near the orthoclase endmember at compositions ~91.1 – 97.4 % orthoclase and 2 samples with ~70 % orthoclase (Figure 15). Activity of sanidine (a_{san}) and albite (a_{ab}) were obtained using Holland's AX program (Holland, 2019). The a_{san} ranges from 0.75 – 0.97 across each location, while a_{ab} is much lower ranging from 0.06 – 0.62, with the highest activities reported from location 2.

Plagioclase compositions were normalized to 8 O (Table 9). This mineral was present in each sample both optically and under the microprobe. Myrmekitic texture between plagioclase and quartz was seen in a few of the samples. Samples from locations 1 and 2 have andesine compositions, those from locations 3 and 4 have oligoclase compositions. Two samples from location 4 had compositions near the albite end-

member which indicates that these were altered during metamorphism (Figure 15). Activities of anorthite and albite were obtained using Holland's AX program (Holland, 2019). The a_{an} ranges from 0.27 – 0.53 with a couple outliers with activities as low as 0.03. The a_{ab} ranges from 0.58 -0.67 in samples from locations 1 and 2, and higher activities of 0.78 – 0.97 in samples from locations 3 and 4.

Clinopyroxene compositions were normalized to 6 O (Table 10). This mineral was prominent in samples from locations 1 and 2 and many grains from here had a subophitic texture. Samples from locations 3 and 4 contained less clinopyroxene which also appeared heavily altered in the samples especially from location 3 where microprobe analyses were not obtained. Compositions of these samples were split between augite and diopside (Figure 16). Activities were obtained using Holland's AX program (Holland, 2019). The most significant activities were from diopside (0.48 0.60) and hedenbergite (0.27 – 0.68) while minor activities of Ca-tschermakite, jadeite and acmite (0.00-0.15 for all three) were found.

Orthopyroxene was normalized to 6 O (Table 11). The samples from the Black Rock Forest showed heavy alteration of this mineral and thus clean minerals to analyze were not as common. Locations 1 and 2 showed the best orthopyroxene samples while locations 3 and 4 contained more altered and less orthopyroxene. Compositions from locations 1, 2, and 4 fell generally between the enstatite and ferrosilite end-members while those from location 3 fell much closer to ferrosilite. Activities were obtained using Holland's AX program (Holland, 2019).The highest a_{en} are seen in locations 1 and 2 with activites of 0.28-0.30, locality 4 still had a reasonable activity albeit lower (0.06 – 0.13), and locality 3 had a very low activity of 0.003. The a_{fs} was highest at locality 3 with an

activity of 0.52, the first 2 localities still containing significant activites ranging from 0.18 – 0.20, and at the last locality very low activities were obtained from 0.00 – 0.03.

Magnetite was normalized to 4 oxygens (Table 12), and because the microprobe does not calculate ferric iron this was calculated in the normalization calculations. This mineral was not seen in every sample but at least one microprobe analysis from each locality was performed. Throughout each sample magnetite was often seen intergrown with ilmenite . Activities of Fe_3O_4 (mt) were obtained using Holland's AX program (Holland, 2019). The a_{mt} were high, being in the range of 0.93 – 0.98 for all samples.

There were minor amounts of other minerals also seen under the microscope and microprobe. Quartz was found throughout most of the samples with the least seen from location 4. Apatite and ilmenite were prevalent throughout all the samples. Chlorite and serpentine were the two main alteration minerals found in all four locations. The presence of chlorite indicates the alteration of biotite in this region (Léger et al., 1996), the biotite was not analyzed in this study but could be seen in some hand samples. Lastly, sulfides (pyrite) were found in some of the samples from locality 1.

Amphiboles were normalized to 24 O (Table 13) using the spreadsheet from Locock (2014). The cations for Fe^{2+}/Fe^{3+} and Mn^{2+}/Mn^{3+} were calculated within this spreadsheet, by seeking electroneutrality by adjusting the valences of Fe and Mn according to one (or more) cation normalization schemes, as the microprobe does not determine these ratios. This spreadsheet also determines the classification of amphibole separating them into groups, subgroups, and species. The samples collected from the Black Rock Forest consist mainly of pargasite with lesser amounts of hastingsite and other amphiboles. All but one sample are part of the O-F-Cl group and Ca subgroup, with

the exception being cummingtonite, which is part of the Mg-Fe-Mn subgroup, was found in location 1. Of the Ca-amphiboles in locations 1 and 2, mainly Mg and Na-rich pargasites were seen, while those collected from locations 3 and 4 were more Fe and K rich. Hastingsites were found in locations 2, 3, and 4. Those from location 2 are more Mg rich and those from 3 and 4 are more K-rich. Other amphibole species found here includes ferritschermakite, magnesiohornblende, potassic-ferri-sadanagaite, cummingonite, and edenite.

The Cl incorporation into these amphiboles increases systematically with increasing ^{T}Al, $^{C}Fe^{2+}$, and ^{A}K (Fig. 17). The graph of X_{Si} (= $^{T}Si/^{T}Al+^{T}Si$) shows the inverse relationship indicating that increasing Cl in the W-site correlates to a slight decrease in Si in the T-site. $^{C}Fe^{2+}$ and K have a positive correlation to increasing Cl content showing that as $^{C}Fe^{2+}$ and K apfu increases so does Cl apfu. Similar patterns have been described in other articles looking at Cl-rich calcic amphiboles (Morrison, 1991; Henry and Daigle, 2018) indicating that ^{T}Al, $^{C}Fe^{2+}$ and K may exert some control on how much Cl is accepted into the amphibole's structure. This correlation indicates that Cl incorporation depends on the subsititution of Fe^{2+} for Mg, ^{T}Al for Si, and K for Na in its crystallographic structure. These substitutions together form an FeAlK index (=Fe# *(^{T}Al +K) (Jenkins, 2019). A plot of Cl APFU vs. this index (Figure 17) has a linear correlation and fits the trend derived in Jenkins (2019).

Table 8: Microprobe Analyses of K-spar

	Sample ID					
Oxide wt%	1b	1m	1v	3a	3e	3k
n	2	2	1	1	1	1
SiO2	63.57 (12)	62.73 (36)	66.75	65.61	66.44	66.66
TiO2	0.01	0.01	0.00	0.03	0.00	0.00
Al2O3	18.60 (4)	18.83	17.97	18.01	17.85	18.62
Cr2O3	0.00	0.01	0.03	0.00	0.00	0.00
Fe2O3	0.00	0.00	0.00	0.00	0.00	0.00
FeO	0.07 (1)	0.02	0.19	0.00	0.00	0.06
MnO	0.01	0.02	0.00	0.00	0.00	0.11
MgO	0.00	0.00	0.03	0.00	0.00	0.00
CaO	0.02	0.03	0.05	0.22	0.02	0.10
Na2O	0.44	0.35	0.24	0.65	0.30	0.88
K2O	15.03 (2)	15.25 (5)	15.58	15.21	15.87	14.63
Total	97.76 (6)	97.25 (29)	100.85	99.72	100.49	101.06
Cations						
Si	3.04	2.98 (1)	3.07	3.04	3.07	3.05
Ti	0.00	0.00	0.00	0.00	0.00	0.00
Al	1.01	1.06	0.98	0.98	0.97	1.00
Cr	0.00	0.00	0.00	0.00	0.00	0.00
Fe3	0.00	0.00	0.00	0.00	0.00	0.00
Fe2	0.00	0.00	0.01	0.00	0.00	0.00
Mn	0.00	0.00	0.00	0.00	0.00	0.00
Mg	0.00	0.00	0.00	0.00	0.00	0.00
Ca	0.00	0.00	0.00	0.01	0.00	0.00
Na	0.04	0.03	0.02	0.06	0.03	0.08
K	0.90	0.93	0.92	0.90	0.93	0.85
Total	5.00	5.00	5.00	5.00	5.00	5.00
a_{san}	0.96	0.96	0.97	0.93	0.97	0.91
a_{ab}	0.12	0.09	0.06	0.17	0.08	0.23

Table 8: Microprobe Analysis of K-spar in the Black Rock Forest (cont)

	Sample ID				
Oxide wt%	4a	4c	4e	4f	4h
n	1	1	2	1	1
SiO2	64.91	66.89	65.08 (6)	67.52	67.63
TiO2	0.09	0.00	0.02	0.03	0.00
Al2O3	19.02	18.56	19.04 (3)	18.17	18.76
Cr2O3	0.07	0.01	0.00	0.03	0.01
Fe2O3	0.00	0.00	0.00	0.00	0.00
FeO	0.00	0.12	0.02	0.06	0.13
MnO	0.00	0.00	0.04	0.00	0.03
MgO	0.00	0.00	0.00	0.00	0.00
CaO	0.14	0.02	0.20 (2)	0.04	0.14
Na2O	2.84	0.53	1.38 (15)	0.33	3.03
K2O	12.29	15.21	14.52 (21)	15.66	11.89
Total	99.36	101.33	100.30 (48)	101.84	101.62
Cations					
Si	2.98	3.06	2.99	3.08	3.04
Ti	0.00	0.00	0.00	0.00	0.00
Al	1.03	1.00	1.03	0.98	1.00
Cr	0.00	0.00	0.00	0.00	0.00
Fe3	0.00	0.00	0.00	0.00	0.00
Fe2	0.00	0.00	0.00	0.00	0.00
Mn	0.00	0.00	0.00	0.00	0.00
Mg	0.00	0.00	0.00	0.00	0.00
Ca	0.01	0.00	0.01	0.00	0.01
Na	0.25	0.05	0.12 (1)	0.03	0.26
K	0.72	0.89	0.85 (1)	0.91	0.68
Total	5.00	5.00	5.00	5.00	5.00
a_{san}	0.82	0.95	0.87	0.97	0.75
a_{ab}	0.46	0.14	0.33	0.09	0.62

Table 9: Microprobe Analyses of Plagioclase in the Black Rock Forest

	Sample ID						
Oxides	1b	1m	1v	2l	2r	2t	2v
n	3	2	2	1	1	1	4
SiO2	58.36 (6)	59.92 (25)	59.78 (7)	60.13	60.01	57.28	56.42 (11)
TiO2	0.02	0.00	0.00	0.02	0.01	0.00	0.02
Al2O3	25.65 (3)	25.48 (2)	25.43	25.90	26.61	26.79	26.75 (1)
Cr2O3	0.00	0.01	0.03	0.00	0.00	0.03	0.01
FeO	0.13 (1)	0.07 (1)	0.16	0.09	0.17	0.04	0.11
MgO	0.01	0.01	0.04 (1)	0.00	0.00	0.00	0.05
MnO	0.01	0.08	0.00	0.11	0.05	0.00	0.02
CaO	6.97 (1)	6.80 (2)	6.41 (1)	7.88	8.45	7.70	8.26 (1)
Na2O	7.17 (1)	7.40 (3)	7.64	7.01	6.67	6.49	6.30 (5)
K2O	0.68 (2)	0.68 (2)	0.48 (1)	0.37	0.31	0.33	0.41
F	0.00	0.00	0.00	0.00	0.00	0.00	0.00
Cl	0.00	0.00	0.00	0.01	0.00	0.01	0.01
Total	99.00 (8)	100.47 (29)	99.98 (8)	101.50	102.28	98.67	98.36 (8)
Cations							
Si	2.63	2.66	2.66	2.65	2.63	2.60	2.57
Ti	0.00	0.00	0.00	0.00	0.00	0.00	0.00
Al	1.36	1.33	1.34	1.35	1.38	1.43	1.44
Cr	0.00	0.00	0.00	0.00	0.00	0.00	0.00
Fe3	0.00	0.00	0.01	0.00	0.00	0.00	0.00
Fe2	0.00	0.00	0.00	0.00	0.01	0.00	0.00
Mn	0.00	0.00	0.00	0.00	0.00	0.00	0.00
Mg	0.00	0.00	0.00	0.00	0.00	0.00	0.00
Ca	0.34	0.32	0.31	0.37	0.40	0.37	0.40
Na	0.63	0.64	0.66	0.60	0.57	0.57	0.56
K	0.04	0.04	0.03	0.02	0.02	0.02	0.02
Total	5.00	5.00	5.00	5.00	5.00	5.00	5.00
a_{an}	0.44	0.43	0.41	0.49	0.53	0.51	0.53
a_{ab}	0.63	0.65	0.67	0.61	0.59	0.60	0.58

Table 9: Microprobe Analyses of Plagioclase in the Black Rock Forest (cont)

	Sample ID			
Oxides	3a	3e	3k	3r
n	5	2	1	1
SiO2	64.53 (22)	62.81 (35)	64.58	63.35
TiO2	0.03	0.02	0.00	0.00
Al2O3	23.73 (11)	23.30 (1)	22.98	23.32
Cr2O3	0.02	0.01	0.00	0.01
FeO	0.18 (2)	0.01	0.08	0.00
MgO	0.02	0.00	0.00	0.00
MnO	0.03	0.00	0.00	0.02
CaO	4.75 (16)	4.34 (1)	4.65	4.63
Na2O	9.30 (14)	9.45 (1)	9.10	9.10
K2O	0.12	0.10	0.21	0.11
F	0.00	0.00	0.00	0.00
Cl	0.01	0.28 (4)	0.00	0.00
Total	102.71 (19)	100.27 (30)	101.61	100.54
Cations				
Si	2.78	2.77 (1)	2.82	2.79
Ti	0.00	0.00	0.00	0.00
Al	1.21 (1)	1.21	1.18	1.21
Cr	0.00	0.00	0.00	0.00
Fe3	0.00	0.00	0.00	0.00
Fe2	0.00	0.00	0.00	0.00
Mn	0.00	0.00	0.00	0.00
Mg	0.00	0.00	0.00	0.00
Ca	0.22 (1)	0.21	0.22	0.22
Na	0.78 (1)	0.81	0.77	0.78
K	0.01	0.01	0.01	0.01
Total	5.00	5.00	5.00	5.00
a_{an}	0.29	0.27	0.29	0.29
a_{ab}	0.78	0.80	0.78	0.78

Table 9: Microprobe Analyses of Plagioclase in the Black Rock Forest (cont)

	Sample ID				
Oxides	4a	4c	4e	4f	4h
n	2	1	3	1	1
SiO2	64.55 (15)	70.94	65.37 (7)	61.75	72.05
TiO2	0.01	0.03	0.00	0.01	0.00
Al2O3	23.01 (24)	20.42	23.38 (3)	24.26	19.61
Cr2O3	0.00	0.00	0.02	0.00	0.05
FeO	0.21 (2)	0.13	0.07 (1)	0.15	0.00
MgO	0.00	0.05	0.01	0.10	0.01
MnO	0.02	0.01	0.09	0.02	0.04
CaO	4.94 (13)	0.42	4.76 (3)	4.98	0.56
Na2O	8.41	11.22	8.96 (1)	8.55	11.48
K2O	0.14 (1)	0.42	0.23 (2)	0.39	0.06
F	0.00	0.00	0.00	0.00	0.00
Cl	0.01	0.01	0.01	0.01	0.08
Total	101.30 (25)	103.64	102.91 (6)	100.20	103.90
Cations					
Si	2.84 (1)	3.01	2.82	2.73	3.05
Ti	0.00	0.00	0.00	0.00	0.00
Al	1.19 (1)	1.02	1.19	1.26	0.98
Cr	0.00	0.00	0.00	0.00	0.00
Fe3	0.00	0.00	0.00	0.01	0.00
Fe2	0.01	0.00	0.00	0.00	0.00
Mn	0.00	0.00	0.00	0.00	0.00
Mg	0.00	0.00	0.00	0.01	0.00
Ca	0.23	0.02 (1)	0.22	0.24	0.03
Na	0.72	0.92	0.75	0.73	0.94
K	0.01	0.02	0.01	0.02	0.00
Total	5.00	5.00	5.00	5.00	5.00
a_{an}	0.32	0.03	0.30	0.32	0.04
a_{ab}	0.75	0.96	0.77	0.74	0.97

Table 10: Microprobe Analyses of Clinopyroxene

	Sample ID					
	1b	1v	2l	2r	2t	2v
n	6	1	3	2	2	1
SiO2	49.33 (38)	53.76	48.40 (62)	53.21 (8)	52.57 (4)	49.53
TiO2	0.15 (1)	0.15	0.82 (11)	0.11 (1)	0.28 (1)	0.18
Al2O3	3.99 (3)	1.45	4.94 (53)	1.63 (4)	2.34 (4)	1.97
Cr2O3	0.00	0.04	0.01	0.01	0.02	0.05
FeO	14.62 (39)	11.24	12.68 (33)	12.17 (22)	11.16 (5)	10.73
MgO	12.48 (12)	12.00	11.61 (14)	12.53 (13)	11.73 (1)	11.10
MnO	0.24 (1)	0.18	0.39 (1)	0.32	0.52 (1)	0.45
CaO	15.52 (61)	21.74	17.76 (58)	17.36 (54)	20.73	21.56
Na2O	0.43 (2)	0.48	0.89 (6)	0.28 (2)	0.58 (1)	0.55
K2O	0.05	0.00	0.35 (6)	0.00	0.01	0.00
F	0.00	0.05	0.03	0.06 (1)	0.00	0.00
Cl	0.01	0.00	0.13 (2)	0.03	0.01	0.00
Total	96.81 (28)	101.06	97.97 (33)	97.68 (18)	99.95 (7)	96.12
Si	1.93 (1)	2.02	1.88 (2)	2.07 (1)	2.00	1.96
Ti	0.00	0.00	0.00	0.00	0.00	0.00
Al	0.19 (2)	0.06	0.23 (3)	0.07	0.10	0.09
Cr	0.00	0.00	0.00	0.00	0.00	0.00
Fe3	0.00	0.00	0.00	0.00	0.00	0.00
Fe2	0.48 (2)	0.35	0.42 (1)	0.40 (1)	0.35	0.35
Mn	0.01	0.01	0.01	0.01	0.02	0.02
Mg	0.73 (1)	0.67	0.67 (1)	0.73 (1)	0.66	0.65
Ca	0.65 (3)	0.87	0.74 (2)	0.72 (2)	0.84	0.91
Na	0.01	0.01	0.01	0.00	0.01	0.01
Total	4.00	3.99	3.97	4.00	3.99	3.99
a_{di}	0.50	0.57	0.53	0.52	0.54	0.60
a_{hed}	0.34	0.32	0.27	0.31	0.31	0.30
a_{cats}	0.15	0.00	0.11	0.00	0.11	0.05
a_{jd}	0.03	0.03	0.03	0.02	0.04	0.01
a_{acm}	0.00	0.00	0.02	0.00	0.00	0.02

Table 10: Microprobe Analyses of Clinopyroxene (cont)			
	Sample ID		
	4a	4c	4e
n	1	1	2
SiO2	51.41	52.59	52.39 (5)
TiO2	0.21	0.15	0.09
Al2O3	1.65	1.54	1.45 (8)
Cr2O3	0.00	0.00	0.00
FeO	14.83	22.15	23.83 (5)
MgO	9.34	9.40	8.84 (7)
MnO	0.47	0.32	0.31 (1)
CaO	21.02	12.28	11.01 (12)
Na2O	0.47	0.31	0.16 (1)
K2O	0.01	0.14	0.10
F	0.00	0.15	0.19 (1)
Cl	0.01	0.13	0.01
Total	99.40	99.06	98.30 (12)
Si	2.00	2.09	2.11
Ti	0.00	0.00	0.00
Al	0.08	0.07	0.07
Cr	0.00	0.00	0.00
Fe3	0.00	0.00	0.00
Fe2	0.48	0.74	0.80
Mn	0.02	0.01	0.01
Mg	0.54	0.56	0.53
Ca	0.88	0.52	0.48 (1)
Na	0.01	0.00	0.00
Total	3.99	4.00	4.00
a_{di}	0.48	0.48	0.58
a_{hed}	0.42	0.54	0.68
a_{cats}	0.08	0.00	0.00
a_{jd}	0.02	0.03	0.03
a_{acm}	0.00	0.00	0.00

*Location 3 had visible clinopyroxene in a few rocks but electron microprobe analyses could not be obtained on them.

Table 11: Microprobe Analyses of Orthopyroxene

	Sample ID					
	1v	2l	2r	2t	2v	3k
n	2	2	1	1	3	1
SiO2	50.9 (19)	52.2 (17)	53.3	54.0	53.4 (7)	41.8
TiO2	0.05 (1)	0.06 (1)	0.08	0.05	0.05	0.01
Al2O3	0.96 (1)	0.88 (2)	1.04	0.82	0.95 (1)	6.83
Cr2O3	0.03	0.01	0.00	0.00	0.00	0.00
FeO	26.9 (2)	26.4 (7)	27.2	26.3	27.5 (1)	34.8
MgO	17.8 (1)	18.6 (8)	18.7	18.7	18.7 (4)	1.16
MnO	0.90	0.98 (1)	1.06	0.98	0.93 (1)	0.88
CaO	0.63	0.64 (1)	0.55	0.55	0.60	0.10
Na2O	0.04	0.00	0.04	0.10	0.03	0.10
K2O	0.00	0.00	0.00	0.01	0.00	1.27
F	0.10 (1)	0.12 (2)	0.00	0.19	0.08 (1)	0.17
Cl	0.00	0.00	0.00	0.00	0.00	0.00
Total	98.2 (24)	99.7 (33)	101.9	101.6	102.1 (10)	87.0
SiO2	1.99	2.00	2.00	2.03	2.00	2.05
TiO2	0.00	0.00	0.00	0.00	0.00	0.00
Al2O3	0.04	0.04	0.05	0.04	0.04	0.39
Cr2O3	0.00	0.00	0.00	0.00	0.00	0.00
Fe2O3	0.00	0.00	0.00	0.00	0.00	0.00
FeO	0.88	0.84	0.85	0.83	0.86	1.43
MnO	0.03	0.03	0.03	0.03	0.03	0.04
MgO	1.03	1.06	1.04	1.05	1.04	0.08
CaO	0.03	0.03	0.02	0.02	0.02	0.01
Na2O	0.00	0.00	0.00	0.00	0.00	0.00
total	4.00	4.00	4.00	4.00	4.00	4.00
a_{en}	0.28	0.30	0.29	0.28	0.29	0.00
a_{fs}	0.20	0.19	0.19	0.18	0.19	0.52
a_{mgts}	0.02	0.02	0.02	0.00	0.02	0.00

Table 12: Microprobe analyses of magnetite

	Sample ID				
	1b-mt1	mt2v-1	mt3e-1	mt4f-1	mt4h-1
N	1	1	1	1	1
Si	0.00	0.00	0.13	0.00	0.00
Ti	0.02	0.00	0.01	0.01	0.02
Al	0.00	0.01	0.02	0.00	0.00
Fe3+	1.96	1.97	1.68	1.95	1.93
Fe2+	0.00	0.00	0.00	0.00	0.00
Fe2+	1.01	0.99	1.09	1.00	1.02
Mg	0.00	0.00	0.01	0.00	0.00
Mn2+	0.00	0.00	0.00	0.00	0.00
Ni	0.00	0.00	0.00	0.00	0.00
Ca	0.00	0.00	0.02	0.00	0.00
Total Cations	3.00	2.97	2.96	2.97	2.98
a_{mt}	0.96	0.98	0.93	0.98	0.96

Table 13: Microprobe Analyses of Amphibole in the Black Rock Forest

	Sample ID					
Oxide wt %	1b -core	1b-rim	1m-core	1m-rim	1v-core	1v-rim
n	4	2	7	3	7	7
SiO2	43.7 (5)	44.2 (19)	42.3 (14)	42.5 (9)	42.5 (13)	41.8 (14)
TiO2	2.34	2.38 (2)	1.97 (9)	2.15 (2)	2.32 (2)	2.30 (2)
Al2O3	10.8 (2)	10.3 (15)	11.1 (3)	11.3	11.1 (2)	11.3 (5)
Cr2O3	0.06	0.04	0.04	0.01	0.02	0.03
FeO	17.2 (4)	16.7 (2)	18.4 (24)	17.1 (3)	17.3 (7)	17.2 (6)
MgO	10.2 (3)	10.3 (6)	10.4 (16)	10.1 (5)	9.74 (4)	9.46 (5)
MnO	0.11 (1)	0.10 (1)	0.22 (1)	0.19 (1)	0.18	0.13 (1)
CaO	11.6 (2)	11.4 (3)	10.5 (21)	11.3 (2)	11.1 (3)	11.3 (3)
Na2O	1.66	1.25 (3)	1.45 (6)	1.47 (1)	1.64 (1)	1.55 (1)
K2O	1.64	1.45 (2)	1.46 (6)	1.72 (1)	1.67 (1)	1.74 (1)
F	0.23 (1)	0.14 (1)	0.22 (1)	0.25 (1)	0.24 (1)	0.25 (1)
Cl	0.39	0.30 (1)	0.45 (2)	0.53	0.55	0.55
Total	99.7 (7)	98.4 (2)	98.3 (12)	98.4 (12)	98.1 (19)	97.4 (16)
Cations						
^{T}Si	6.27 (4)	6.44 (4)	6.33 (2)	6.40	6.42 (1)	6.38 (1)
^{T}Al	1.55 (1)	1.56 (4)	1.65 (1)	1.60	1.57 (1)	1.62 (1)
^{T}Ti	0.06 (1)	0.00	0.00	0.00	0.00	0.00
^{T}Fe3+	0.12 (2)	0.00	0.02	0.00	0.84 (12)	0.00
Σ T	8.00	8.00	8.00	8.00	8.00	8.00
^{C}Ti	0.26	0.26	0.22 (1)	0.24	0.26	0.26
^{C}Al	0.36	0.21 (2)	0.31 (2)	0.40	0.40	0.42
^{C}Cr	0.01	0.00	0.00	0.00	0.00	0.01
^{C}Mn3+	0.12 (2)	0.00	0.00	0.00	0.00	0.00
^{C}Fe3+	0.40 (7)	0.52 (6)	0.44 (8)	0.14	0.11	0.10 (1)
^{C}Mn2+	0.30 (6)	0.00	0.00	0.00	0.01	0.01
^{C}Fe2+	2.03 (1)	1.03 (12)	1.70 (8)	1.95 (1)	2.03 (1)	2.07 (1)
^{C}Mg	2.18 (2)	2.98 (9)	2.33 (3)	2.26 (1)	2.20 (1)	2.15 (1)
Σ C	5.00	5.00	5.00	5.00	5.00	5.00
^{B}Mn2+	0.06 (1)	0.01	0.03	0.02	0.02	0.02
^{B}Fe2+	0.02	0.06 (1)	0.19 (4)	0.06	0.05	0.05
^{B}Mg	0.00	0.00	0.02	0.00	0.00	0.00
^{B}Ca	1.78 (1)	1.77 (1)	1.67 (4)	1.82	1.81	1.84
^{B}Na	0.14	0.15	0.10	0.10	0.13	0.11
Σ B	2.00	2.00	2.00	2.00	2.00	2.00
^{A}Ca	0.00	0.00	0.00	0.00	0.00	0.00
^{A}Na	0.32 (1)	0.20	0.31 (1)	0.33	0.35	0.35
^{A}K	0.30	0.27	0.27	0.33	0.32	0.34
Σ A	0.62	0.46	0.58	0.66	0.67	0.69
Total	15.6 (1)	15.5 (1)	15.6 (3)	15.7	15.7	15.7
Anions						
OH	1.8	1.9 (1)	1.8 (1)	1.8	1.75	1.74
F	0.10	0.06	0.10	0.12	0.11	0.12
Cl	0.10	0.07	0.11 (1)	0.13	0.14	0.14
Σ OH+F+Cl	2.00	2.00	2.00	2.00	2.00	2.00
a_{KCH}	0.000304	0.0001620	0.000668	0.000434	0.000435	0.000444

Table 13: Microprobe Analyses of Amphibole in the Black Rock Forest (cont.)

	Sample ID			
Oxide wt %	2l-core	2l-rim	2r-core	2r-rim
n	6	6	7	7
SiO2	44.2 (7)	44.0 (7)	44.9 (5)	44.9 (7)
TiO2	2.12 (2)	2.11 (2)	2.19 (1)	2.11 (1)
Al2O3	10.7 (2)	11.0 (4)	10.7 (3)	10.8 (2)
Cr2O3	0.03	0.04	0.01	0.01
FeO	16.5 (1)	16.6 (1)	16.8 (2)	16.7 (6)
MgO	10.4 (3)	10.0 (5)	10.4 (2)	10.5 (4)
MnO	0.21 (2)	0.23 (4)	0.25 (1)	0.18 (1)
CaO	11.5 (2)	11.0 (9)	11.5 (2)	11.6 (2)
Na2O	1.60 (2)	1.58 (1)	1.66 (1)	1.54 (1)
K2O	1.05 (1)	1.00 (1)	1.04 (1)	1.08 (1)
F	0.14 (1)	0.08 (1)	0.13	0.09 (1)
Cl	0.36	0.36	0.36	0.35
Total	98.6 (6)	97.9 (14)	99.8 (5)	99.7 (11)
Cations				
^{T}Si	6.55 (1)	6.58	6.59 (1)	6.59
^{T}Al	1.45 (1)	1.42	1.41 (1)	1.41
^{T}Ti	0.00	0.00	0.00	0.00
^{T}Fe3+	0.00	0.00	0.00	0.00
Σ T	8.00	8.00	8.00	8.00
^{C}Ti	0.24	0.23	0.24	0.23
^{C}Al	0.46 (1)	0.46 (1)	0.44	0.45
^{C}Cr	0.00	0.00	0.00	0.00
^{C}Mn3+	0.00	0.00	0.00	0.00
^{C}Fe3+	0.14 (1)	0.08	0.09	0.10
^{C}Mn2+	0.00	0.01	0.00	0.00
^{C}Fe2+	1.92 (1)	1.91	1.95 (1)	1.92 (1)
^{C}Mg	2.23 (1)	2.31	2.27	2.29 (1)
Σ C	5.00	5.00	5.00	5.00
^{B}Mn2+	0.03	0.02	0.03	0.02
^{B}Fe2+	0.05 (1)	0.02	0.02	0.03
^{B}Mg	0.00	0.0	0.00	0.00
^{B}Ca	1.77 (1)	1.84	1.81	1.82
^{B}Na	0.15 (1)	0.11	0.14	0.12
Σ B	2.00	2.00	2.00	2.00
^{A}Ca	0.00	0.00	0.00	0.00
^{A}Na	0.33 (1)	0.33	0.33 (1)	0.31
^{A}K	0.19	0.20	0.19	0.20
Σ A	0.52 (1)	0.5	0.53	0.52
Total	15.5 (1)	15.5	15.5	15.5
Anions				
OH	1.86	1.9	1.85	1.87
F	0.06	0.05	0.06	0.06
Cl	0.09	0.09	0.09	0.09
Σ OH+F+Cl	2.00	2.0	2.00	2.02
a_{KCH}	0.000213	0.000226	0.000201	0.000201

Table 13: Microprobe Analyses of Amphibole in the Black Rock Forest (cont.)

	Sample ID			
Oxide wt %	2t-core	2t-rim	2v-core	2v-rim
n	7	3	6	6
SiO2	44.4 (7)	45.8 (21)	42.5 (14)	42.64 (11)
TiO2	2.17 (1)	1.44 (11)	2.06 (1)	2.01 (1)
Al2O3	10.9 (1)	8.9 (32)	11.1 (3)	11.29 (2)
Cr2O3	0.01	0.05	0.01	0.02
FeO	16.8 (4)	15.7 (12)	17.9 (4)	17.74 (7)
MgO	10.4 (2)	11.4 (14)	9.74 (1)	9.71 (2)
MnO	0.21 (1)	0.23 (1)	0.28 (3)	0.21 (3)
CaO	11.4 (2)	12.9 (25)	11.5 (2)	11.54 (3)
Na2O	1.70 (2)	1.11 (6)	1.66 (1)	1.49 (1)
K2O	1.03	0.69 (6)	1.33	1.44 (1)
F	0.10 (1)	0.13 (2)	0.15 (1)	0.14 (1)
Cl	0.35	0.23 (2)	0.56	0.59
Total	99.3 (15)	98.5 (10)	98.8 (19)	98.8 (14)
Cations				
^{T}Si	6.59 (1)	6.66 (1)	6.40 (1)	6.41 (1)
^{T}Al	1.41 (1)	1.26 (3)	1.60 (1)	1.60 (1)
^{T}Ti	0.00	0.08 (1)	0.00	0.00
^{T}Fe3+	0.00	0.00	0.00	0.00
Σ T	8.00	8.00	8.00	8.00
^{C}Ti	0.21 (1)	0.16 (1)	0.23	0.23
^{C}Al	0.48 (1)	0.31 (3)	0.37 (1)	0.40 (1)
^{C}Cr	0.00	0.01	0.00	0.00
^{C}Mn3+	0.00	0.00	0.00	0.00
^{C}Fe3+	0.11	0.08 (1)	0.16 (2)	0.18
^{C}Mn2+	0.00	0.01	0.00	0.00
^{C}Fe2+	1.93	1.85	2.05 (1)	2.01 (1)
^{C}Mg	2.27	2.53 (3)	2.18 (1)	2.17
Σ C	5.00	4.94 (1)	5.00	5.00 (1)
^{B}Mn2+	0.02	0.02	0.03	0.03
^{B}Fe2+	0.03	0.05	0.05	0.05
^{B}Mg	0.00	0.00	0.00	0.00
^{B}Ca	1.80	1.88 (1)	1.85	1.86
^{B}Na	0.14	0.08 (1)	0.07	0.08
Σ B	2.00	2.00	2.00	2.00
^{A}Ca	0.00	0.19 (3)	0.00	0.00
^{A}Na	0.35 (1)	0.24 (1)	0.41	0.36
^{A}K	0.19	0.13 (1)	0.26	0.28
Σ A	0.54 (1)	0.56 (1)	0.67	0.63
Total	15.5 (1)	15.5	15.67	15.63 (1)
Anions				
OH	1.87	1.88 (1)	1.78	1.79
F	0.05	0.06 (1)	0.07	0.08
Cl	0.09	0.06	0.14	0.15
Σ OH+F+Cl	2.01	2.00	2.00	2.00
a_{KCH}	0.000245	0.0000829	0.000822	0.000765

Table 13: Microprobe Analyses of Amphibole in the Black Rock Forest

	Sample ID			
Oxide wt %	3a-core	3a-rim	3e-core	3e-rim
n	10	8	8	3
SiO2	37.7 (17)	37.8 (21)	36.6 (42)	38.0 (2)
TiO2	2.50 (3)	2.57 (2)	1.92 (5)	1.36 (5)
Al2O3	11.7 (3)	11.6 (2)	10.9 (17)	12.1 (1)
Cr2O3	0.02	0.00	0.01	0.01
FeO	28.9 (4)	28.3 (3)	27.4 (8)	28.3 (11)
MgO	2.53 (1)	2.49 (2)	3.50 (5)	3.12 (7)
MnO	0.27 (1)	0.21 (1)	0.39 (1)	0.47 (1)
CaO	10.5 (4)	10.6 (4)	10.2 (2)	10.3 (4)
Na2O	1.68 (2)	1.65 (1)	1.81 (2)	1.77 (1)
K2O	2.31 (1)	2.33 (1)	2.07 (2)	2.35 (2)
F	0.21 (1)	0.20 (1)	0.33 (2)	0.40 (1)
Cl	2.91 (2)	2.86 (2)	2.47 (5)	2.98 (6)
Total	100.5 (27)	99.9 (27)	97.0 (66)	100.4 (118)
Cations				
^{T}Si	6.05 (1)	6.05 (2)	6.15 (3)	6.18
^{T}Al	1.95 (1)	1.95 (2)	1.74 (1)	1.82
^{T}Ti	0.00	0.00	0.04 (1)	0.00
^{T}Fe3+	0.00	0.00	0.07 (2)	0.00
Σ T	8.00	8.00	8.00	8.00
^{C}Ti	0.30	0.30	0.20 (1)	0.17 (1)
^{C}Al	0.27 (1)	0.29 (1)	0.41 (2)	0.50
^{C}Cr	0.00	0.00	0.00	0.00
^{C}Mn3+	0.00	0.00	0.00	0.00
^{C}Fe3+	0.28 (2)	0.25 (3)	0.21 (3)	0.21 (1)
^{C}Mn2+	0.00	0.00	0.45 (1)	0.37 (1)
^{C}Fe2+	3.54 (1)	3.58 (2)	3.61 (2)	3.64 (1)
^{C}Mg	0.60	0.59	0.10	0.12
Σ C	5.00	5.00	4.97 (1)	5.00
^{B}Mn2+	0.04	0.03	0.05	0.06
^{B}Fe2+	0.05	0.04	0.00	0.00
^{B}Mg	0.00	0.00	0.00	0.00
^{B}Ca	1.81	1.83	1.83 (1)	1.80 (1)
^{B}Na	0.10	0.10	0.12 (1)	0.14
Σ B	2.00	2.00	2.00	2.00
^{A}Ca	0.00	0.00	0.02 (1)	0.00
^{A}Na	0.42	0.43	0.47 (1)	0.42
^{A}K	0.47	0.48	0.45	0.49 (1)
Σ A	0.89	0.91	0.94 (2)	0.91
Total	15.9	15.9	15.9 (1)	15.9
Anions				
OH	1.10 (1)	1.08 (1)	1.12 (1)	0.98 (1)
F	0.11	0.12	0.17 (1)	0.20
Cl	0.79 (1)	0.80	0.71 (1)	0.82 (2)
Σ OH+F+Cl	2.00	2.00	2.00	2.00
a_{KCH}	0.0405	0.0390	0.0508	0.0445

Table 13: Microprobe Analyses of Amphibole in the Black Rock Forest (cont.)

	Sample ID			
Oxide wt %	3k-core	3k-rim	3r-core	3r-rim
n	3	2	4	3
SiO2	38.2 (10)	38.0 (14)	36.9 (8)	36.9 (6)
TiO2	1.70 (5)	1.54 (1)	1.80 (1)	1.94 (1)
Al2O3	11.6 (4)	11.7 (9)	11.9 (3)	12.1 (2)
Cr2O3	0.01	0.00	0.01	0.00
FeO	30.4 (10)	29.5 (13)	29.6 (5)	29.2 (4)
MgO	1.53 (4)	1.45 (2)	2.10 (1)	2.06 (2)
MnO	0.43	0.48	0.61 (1)	0.44 (1)
CaO	10.2 (1)	10.1 (2)	10.1	10.1
Na2O	1.85 (3)	1.71 (3)	1.70 (2)	1.68 (1)
K2O	2.14 (2)	2.42 (5)	2.38 (1)	2.37
F	0.63 (3)	0.49 (7)	0.22 (1)	0.12
Cl	2.45 (11)	3.11 (18)	3.48 (1)	3.63 (2)
Total	100.3 (112)	99.7	99.9 (10)	99.6 (3)
Cations				
^{T}Si	6.17 (1)	6.20 (2)	6.02 (1)	6.06 (1)
^{T}Al	1.83 (1)	1.81 (2)	1.98 (1)	1.94 (1)
^{T}Ti	0.00	0.00	0.00	0.00
^{T}Fe3+	0.00	0.00	0.00	0.00
Σ T	8.00	8.00	8.00	8.00
^{C}Ti	0.21 (1)	0.19	0.21	0.22
^{C}Al	0.38 (1)	0.45	0.29 (1)	0.36
^{C}Cr	0.00	0.00	0.00	0.00
^{C}Mn3+	0.00	0.00	0.00	0.00
^{C}Fe3+	0.27 (1)	0.22	0.50 (2)	0.32 (2)
^{C}Mn2+	0.00	0.01	0.01	0.01
^{C}Fe2+	3.77 (2)	3.78 (1)	3.47 (1)	3.60 (2)
^{C}Mg	0.37 (1)	0.35 (1)	0.50	0.49
Σ C	5.00	5.00	5.00	5.00
^{B}Mn2+	0.06	0.06	0.07	0.05
^{B}Fe2+	0.05	0.02	0.01	0.04
^{B}Mg	0.00	0.00	0.00	0.00
^{B}Ca	1.76	1.77 (1)	1.78	1.81 (1)
^{B}Na	0.13 (1)	0.14 (1)	0.14	0.10
Σ B	2.00	2.00	2.00	2.00
^{A}Ca	0.00	0.00	0.00	0.00
^{A}Na	0.45 (1)	0.40 (1)	0.40	0.40
^{A}K	0.44	0.50 (1)	0.50	0.52
Σ A	0.89	0.90 (1)	0.89	0.92
Total	15.9	15.9 (1)	15.9	15.9
Anions				
OH	1.01 (1)	0.89 (2)	0.92 (1)	0.88 (1)
F	0.32 (2)	0.25 (3)	0.10	0.06
Cl	0.67 (3)	0.86 (5)	0.98 (1)	1.06 (1)
Σ OH+F+Cl	2.00	2.00	2.00	2.00
a_{KCH}	0.0422	0.0365	0.0696	0.0547

Table 13: Microprobe Analyses of Amphibole in the Black Rock Forest (cont.)

	Sample ID					
Oxide wt %	4a-core	4a-rim	4c-core	4c-rim	4e-core	4e-rim
n	5	7	4	1	7	7
SiO2	41.4 (7)	41.4 (7)	40.7 (5)	41.1	38.7 (11)	39.3 (14)
TiO2	2.55 (1)	2.59 (2)	1.97 (9)	2.46	2.71 (2)	2.56 (6)
Al2O3	11.3 (3)	11.5 (3)	11.5 (4)	10.8	11.1 (2)	11.2 (6)
Cr2O3	0.03	0.03	0.02	0.01	0.01	0.02
FeO	21.1 (5)	21.4 (4)	22.9 (8)	22.5	27.3 (9)	27.1 (5)
MgO	6.82 (1)	6.87 (3)	6.32 (3)	6.21	3.28 (3)	3.36 (3)
MnO	0.21 (1)	0.24 (1)	0.29 (1)	0.29	0.32 (1)	0.31 (1)
CaO	11.2 (3)	11.1 (4)	11.0 (3)	11.3	10.6 (2)	10.7 (2)
Na2O	1.92 (2)	1.91 (2)	1.83 (2)	1.86	1.85 (1)	1.74 (2)
K2O	2.06 (1)	2.02 (1)	2.01 (1)	1.95	2.14 (1)	2.16 (1)
F	0.53 (1)	0.57 (1)	0.36 (1)	0.05	0.27 (1)	0.27 (1)
Cl	1.24	1.24 (1)	1.77 (2)	1.57	2.36 (1)	2.25 (2)
Total	99.8 (9)	100.4 (126)	100.1 (55)	99.7	100.0 (15)	100.3 (66)
Cations						
^{T}Si	6.35	6.32	6.30 (1)	6.36	6.18 (1)	6.23 (2)
^{T}Al	1.65	1.68	1.70 (1)	1.64	1.82 (1)	1.77 (2)
^{T}Ti	0.00	0.00	0.00	0.00	0.00	0.00
^{T}Fe3+	0.00	0.00	0.00	0.00	0.00	0.00
Σ T	8.00	8.00	8.00	8.00	8.00	8.00
^{C}Ti	0.29	0.30	0.23 (1)	0.29	0.33	0.31
^{C}Al	0.40 (1)	0.39 (1)	0.39 (1)	0.34	0.27 (1)	0.32 (1)
^{C}Cr	0.01	0.00	0.00	0.00	0.00	0.00
^{C}Mn3+	0.00	0.00	0.00	0.00	0.00	0.00
^{C}Fe3+	0.02	0.05 (1)	0.13 (1)	0.03	0.14 (1)	0.11 (1)
^{C}Mn2+	0.02	0.02	0.00	0.02	0.00	0.00
^{C}Fe2+	2.69 (1)	2.67 (1)	2.80	2.89	3.48 (1)	3.47
^{C}Mg	1.56	1.56	1.46 (1)	1.44	0.78 (1)	0.79 (1)
Σ C	4.98	5.00 (1)	5.00	5.00	5.00	5.00
^{B}Mn2+	0.01	0.02	0.04	0.02	0.04	0.04
^{B}Fe2+	0.00	0.01	0.04	0.00	0.02	0.02
^{B}Mg	0.00	0.00	0.00	0.00	0.00	0.00
^{B}Ca	1.83	1.81 (1)	1.82	1.87	1.82	1.82
^{B}Na	0.15	0.16	0.11	0.12	0.13	0.12
Σ B	2.00	2.00	2.00	2.00	2.00	2.00
^{A}Ca	0.00	0.00	0.00	0.00	0.00	0.00
^{A}Na	0.42 (1)	0.41	0.44 (1)	0.44	0.45	0.42 (1)
^{A}K	0.40	0.39	0.40	0.39	0.44	0.44
Σ A	0.82	0.80	0.84 (1)	0.82	0.88	0.85 (1)
Total	15.8	15.8	15.8 (1)	15.8	15.9 (1)	15.9 (1)
Anions						
OH	1.42	1.40 (1)	1.36 (1)	1.56	1.23 (1)	1.26 (1)
F	0.26	0.28 (1)	0.18	0.02	0.13 (1)	0.13 (1)
Cl	0.32	0.32	0.46 (1)	0.41	0.64 (1)	0.61 (1)
Σ OH+F+Cl	2.00	2.00	2.00	2.00	2.00	2.00
a_{KCH}	0.000542	0.00130	0.00495	0.00128	0.0173	0.0120

Table 13: Microprobe Analyses of Amphibole in the Black Rock Forest (cont.)

	Sample ID			
Oxide wt %	4f-core	4f-rim	4h-core	4h-rim
n	9	6	2	1
SiO2	37.3 (21)	35.5 (44)	38.2 (5)	37.9
TiO2	2.16 (2)	2.12 (5)	2.52 (2)	2.13
Al2O3	11.8 (6)	11.5 (11)	11.5 (1)	12.2
Cr2O3	0.01	0.01	0.02	0.03
FeO	27.8 (5)	27.3 (7)	28.4 (4)	28.3
MgO	2.84 (2)	2.52 (7)	2.67 (2)	2.53
MnO	0.49 (1)	0.45 (1)	0.33 (1)	0.45
CaO	10.3 (6)	9.9 (12)	10.4 (1)	10.4
Na2O	1.70 (1)	1.34 (4)	1.71 (1)	1.69
K2O	2.26 (1)	2.18 (1)	2.28 (4)	2.34
F	0.20 (2)	0.18 (1)	0.12 (1)	0.34
Cl	2.58 (2)	2.41 (6)	2.58 (1)	2.55
Total	98.7 (28)	94.8 (83)	100.1 (159)	100.1
Cations				
^{T}Si	6.13 (2)	6.07 (3)	6.13	6.08
^{T}Al	1.87 (2)	1.933)	1.88	1.92
^{T}Ti	0.00	0.00	0.00	0.00
^{T}Fe3+	0.00	0.00	0.00	0.00
Σ T	8.00	8.00	8.00	8.00
^{C}Ti	0.27	0.28 (1)	0.30	0.26
^{C}Al	0.43 (1)	0.40 (2)	0.30	0.39
^{C}Cr	0.00	0.00	0.00	0.00
^{C}Mn3+	0.00	0.00	0.00	0.00
^{C}Fe3+	0.18 (3)	0.31 (5)	0.18	0.21
^{C}Mn2+	0.35	0.29 (1)	0.00	0.00
^{C}Fe2+	3.67 (1)	3.61 (3)	3.58 (1)	3.54
^{C}Mg	0.12	0.11	0.64	0.61
Σ C	5.00	5.00	5.00	5.00
^{B}Mn2+	0.05	0.07 (1)	0.04	0.06
^{B}Fe2+	0.00	0.00	0.06	0.06
^{B}Mg	0.00	0.00	0.00	0.00
^{B}Ca	1.82 (1)	1.80 (1)	1.80	1.78
^{B}Na	0.14	0.12	0.10	0.10
Σ B	2.00	2.00	2.00	2.00
^{A}Ca	0.00	0.00	0.00	0.00
^{A}Na	0.41 (1)	0.32 (1)	0.43	0.43
^{A}K	0.47	0.47 (1)	0.47	0.48
Σ A	0.88 (1)	0.79 (1)	0.90 (2)	0.90
Total	z15.9 (1)	15.8 (1)	15.9 (2)	15.9
Anions				
OH	1.18 (1)	1.21 (1)	1.24	1.13
F	0.11 (1)	0.10	0.06	0.17
Cl	0.72 (1)	0.69 (1)	0.70	0.69
Σ OH+F+Cl	2.00	2.00	2.00	2.00
a_{KCH}	0.0377	0.0452	0.0247	0.0263

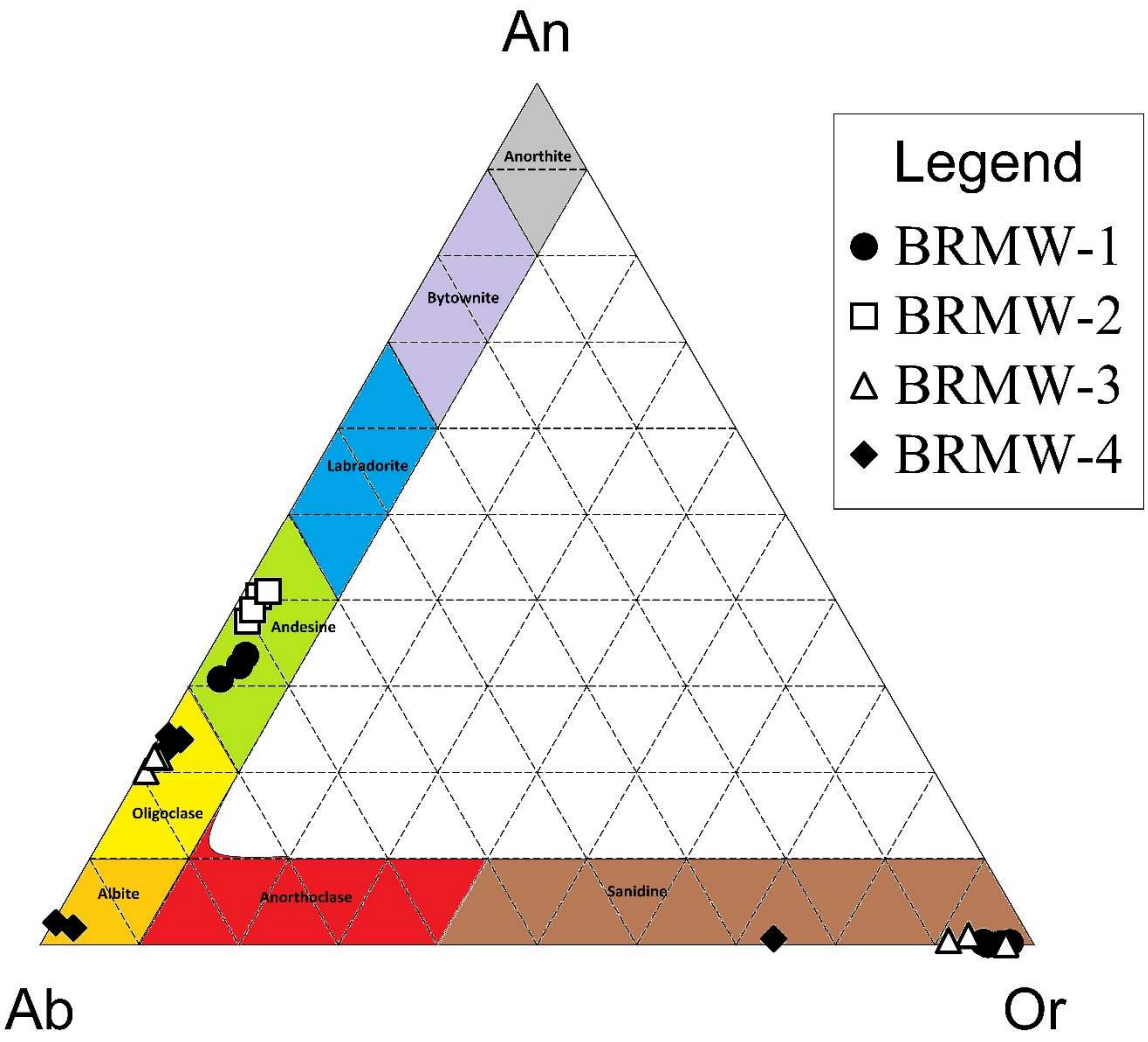


Figure 15: Ternary diagram of feldspars found in four different locations in the Black Rock Forest. Most of the k-spar samples are near end-member orthoclase. The feldspars found near location 1 and 2 are andesine and those from locations 3 and 4 are oligoclase. There are two samples from location 4 which are near the albite endmember.

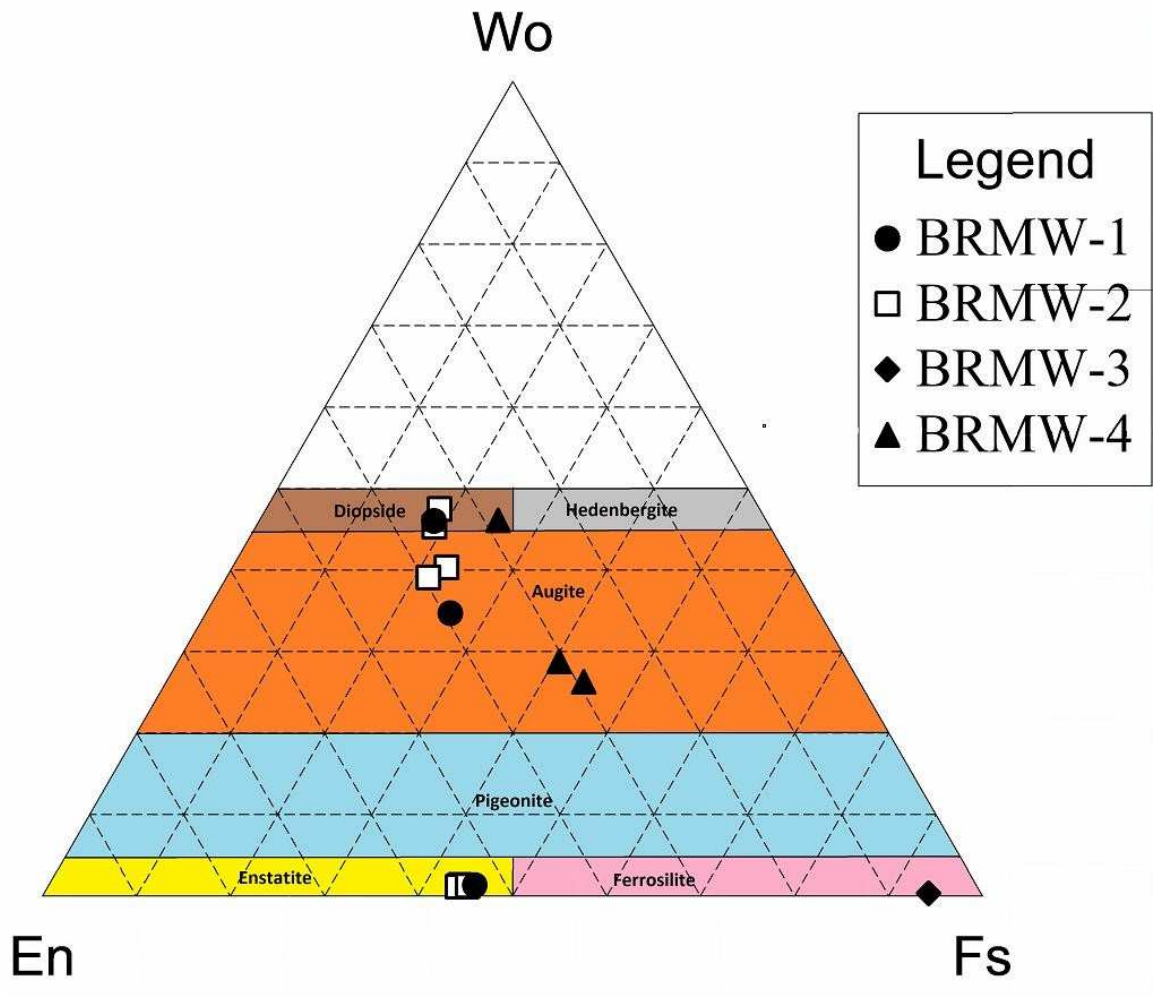


Figure 16: Ternary diagram of pyroxenes found in 4 different locations in the Black Rock Forest. Orthopyroxenes fall closer into the ferrosillite range and most clinopyroxenes were found to be augite.

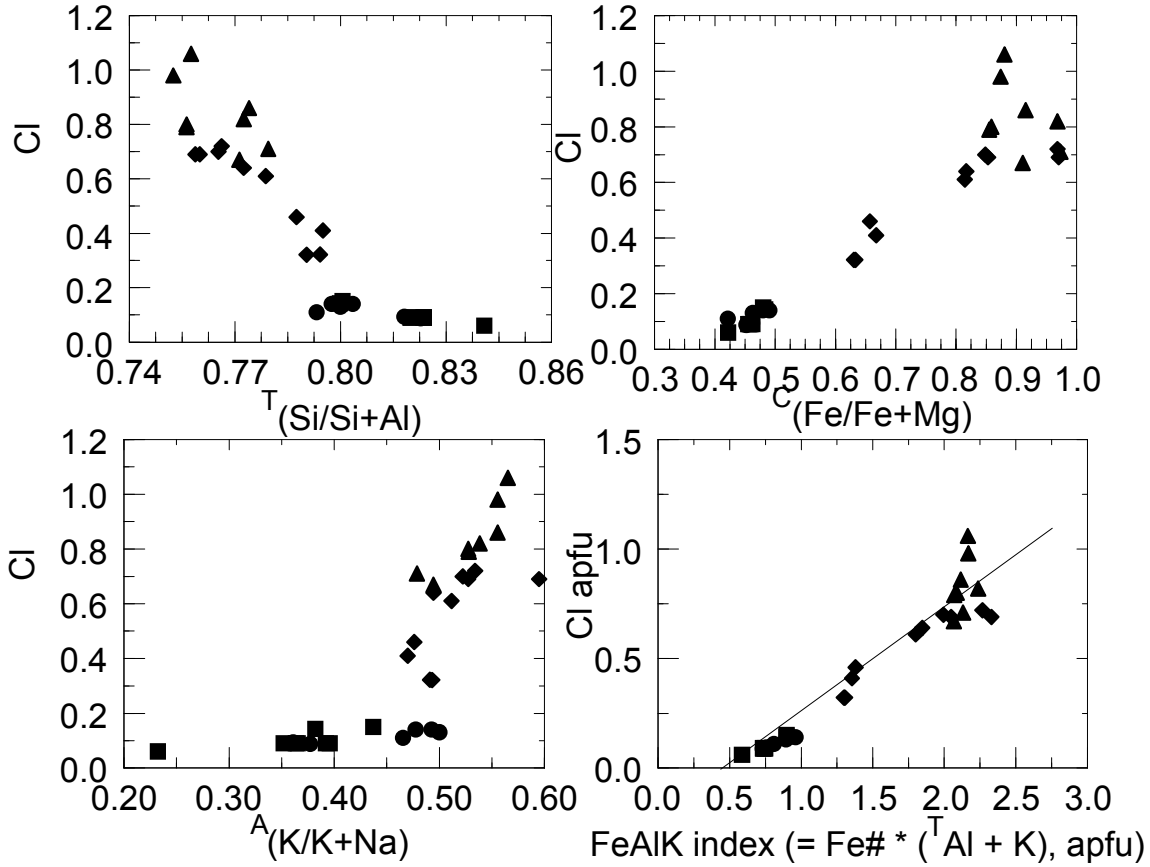


Figure 17: Plots of X_{Si}, X_{Fe2+}, and X_K compared to Cl apfu by location. Location 1 is circles, location 2 is squares, location 3 is triangles, and location 4 is diamonds. The last graph is the Fe# * (^{T}Al+K) plotted against Cl apfu. The trendline is from Jenkins (2019)

Black Rock Forest: metamorphic brine characterization

Ideal activities of the KCH component in the amphiboles from Black Rock Forest were calculated as shown below, because Holland's AX program does not involve Cl-rich hastingsite. The formula used for this calculation is

$$a_{KCH}^{ideal} = 8\,(X_K^A)(X_{Ca}^{M4})^2(X_{Fe}^{M13})^3\left(X_{Fe^{3+}}^{M2}\right)(X_{Al}^{M2})(X_{Al}^{T1})^{0.5}(X_{Si}^{T1})^{0.5}(X_{Cl}^{w})^{\frac{2}{3}} \quad (5)$$

where X_i^j is the mole fraction of cation *i* on site *j*. The site exponents for the K, Ca, and octahedral Fe^{3+}, Fe^{2+}, and Al come directly from the molar coefficients in the formula $KCa_2(Fe_3Fe^{3+})(Al_2Si_6)O_{22}Cl_2$. The site exponents for tetrahedral Si and Al were adopted by Diener et al. (2007) as a means of preventing the activities of the amphibole components from getting so small. The Cl exponent of 2/3 comes from Chan et al. (2016) where 3 activities were tested (Cl, Cl^2, and $Cl^{2/3}$) which showed that $Cl^{2/3}$ had the most consistent K_a values (Chan et al., 2016). In locations 1 and 2 the ideal activity was very low ranging from 0.000162 – 0.000829. This correlates to lower mole fractions for K, Cl, and $^{C}Fe^{2+}$ in these locations. Location 3 had significantly larger activities ranging from 0.0365 – 0.0547. Location 4 was different as activities ranged from 0.000542 – 0.0452. Most of the activities were calculated to be from 0.00130 – 0.0452, while only a couple samples had much lower activities from 0.000542 – 0.00495. The higher activities also correlate to higher mole fractions of K, Cl, and $^{C}Fe^{2+}$ in these locations.

Molality of the Cl can now be calculated to characterize the metamorphic fluids that pervaded through the Black Rock Forest (Table 14). These molalities were calculated with 1 of 5 balanced reactions depending on the minerals present in each sample:

1.0 KCH + 2.0 Qtz = 0.5 An + 0.5 Mt + 1.5 Hed + 0.5 Fs +1.0 FeCl2 + 1.0 Kspar

(8)

1.0 KCH + 3.5 Qtz = 1.0 Kspar + 0.5 An + 1.5 Hed + 1.25 Fs + 1.0 FeCl2 + 0.25 O2

(9)

1.0 KCH + 1.0 Qtz + 0.1667 O2 = 1.0 Kspar + 0.8333 Mt + 0.5 An + 1.0 FeCl2 + 1.5 Hed (10)

1.0 KCH = 1.0 An + 1.0 Hed + 0.5 Mt + 1.0 Fs + 0.5 FeCl2 + 1.0 KCl

(11)

1.0 KCH + 2.0 Qtz + 0.5 FeCl2 = 1.0 Kspar + 0.5 Mt + 0.5 An + 2.0 Fs + 1.5 CaCl2

(12)

Molality of $FeCl_2$ in location 1 was 0.20 - 2.35, in location 2 m $FeCl_2$ was 3.38 - 6.91 which comes from assuming both $FeCl_2$ and KCl are equal. For location 3 molality was 5.37 – 36.4. The calculated molalities, molalities products, and molality ratios are given in Table 14. Plotting these molalities on a geologic map of the Black Rock Forest (figure 19) shows no real pattern of fluid flow. This supports localized heterogeneity in the metamorphic brines that formed these gneisses (Kusebauch et al, 2015).

The salinity of metamorphic brines, especially those rich in Cl, is a factor in the transportation of ore metals and could aid in determining the concentrations of these metals in the rocks. Combining the molality data calculated in this study with graphs of metal-bearing crustal fluids from Yardley and Bodnar (2005), a range of metal concentrations that can be supported by these fluids can be determined (Fig. 18). The fluids for Black Rock Forest could potentially contain concentrations of Fe up to 130,000

ppm, Mn up to 70,000 ppm, Zn up to 120,000 ppm, Pb up to 10,000 ppm, and Cu up to 1,000 ppm.

Table 14: Activities of mineral components and derived molalities for the Black Rock Forest samples

Sample	Rxn #	a_{san}	a_{an}	a_{hed}	a_{fs}	a_{mt}	a_{KCH}	mFeCl2	mKCl	$m(CaCl_2^{1.5}/FeCl_2^{0.5})$	mCl
1b	8	0.96	0.44	0.34	0.20	0.96	0.00	0.12			0.24
1m	10	0.96	0.43	0.34		0.96	0.00	0.10			0.20
1v	9	0.97	0.41	0.32	0.20	0.96	0.00	1.18			2.35
2l	11		0.49	0.27	0.19	0.99	0.00	1.26	1.58		4.09*
2r	11		0.53	0.31	0.19	0.99	0.00	1.13	1.29		3.56*
2t	11		0.51	0.31	0.18	0.99	0.00	1.09	1.19		3.38*
2v	11		0.53	0.30	0.19	0.99	0.00	1.81	3.28		6.91*
3a	12	0.93	0.29		0.52	0.94	0.04			0.03	
3e	12	0.97	0.27		0.52	0.94	0.05			0.04	
3k	12	0.91	0.29		0.52	0.94	0.04			0.03	
3r	12	0.93	0.29		0.52	0.94	0.06			0.05	
4a	9	0.82	0.32	0.42	0.17		0.00	2.69			5.37
4c	9	0.95	0.03	0.54	0.17		0.00	18.20			36.40
4e	9	0.88	0.30	0.70	0.20		0.01	15.58			31.17
4f	10	0.97	0.32	0.42		0.97	0.04	6.31			12.61
4h	10	0.79	0.04	0.42		0.95	0.03	14.46			28.91

* Assuming molalities of $FeCl_2$ and KCl are equal.

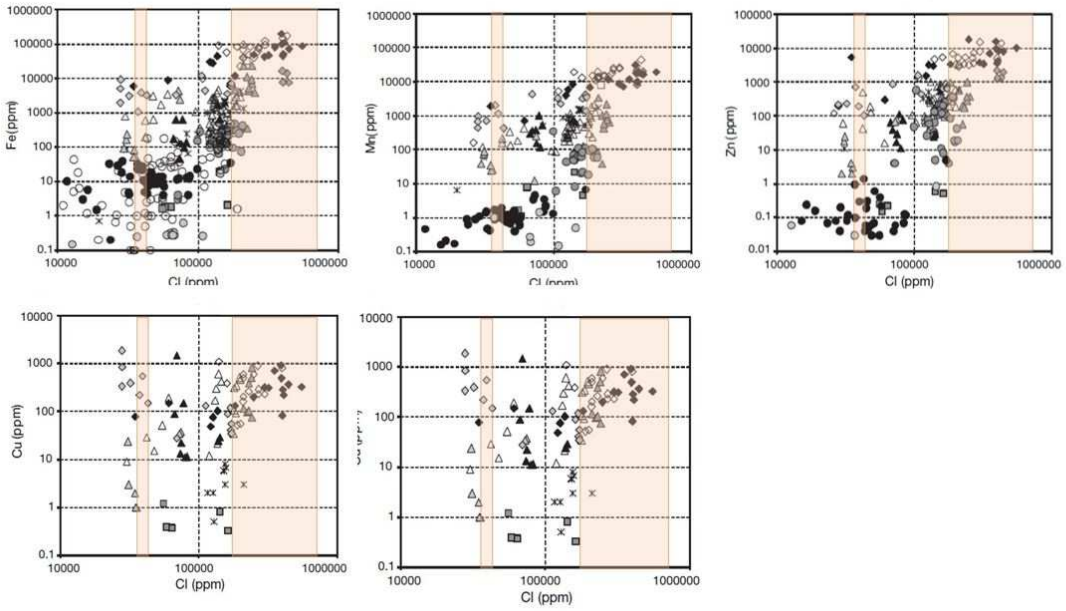


Figure 18: Cl brine concentrations from the Black Rock Forest superimposed on concentrations of metals in crustal fluids (Yardley, 2005).

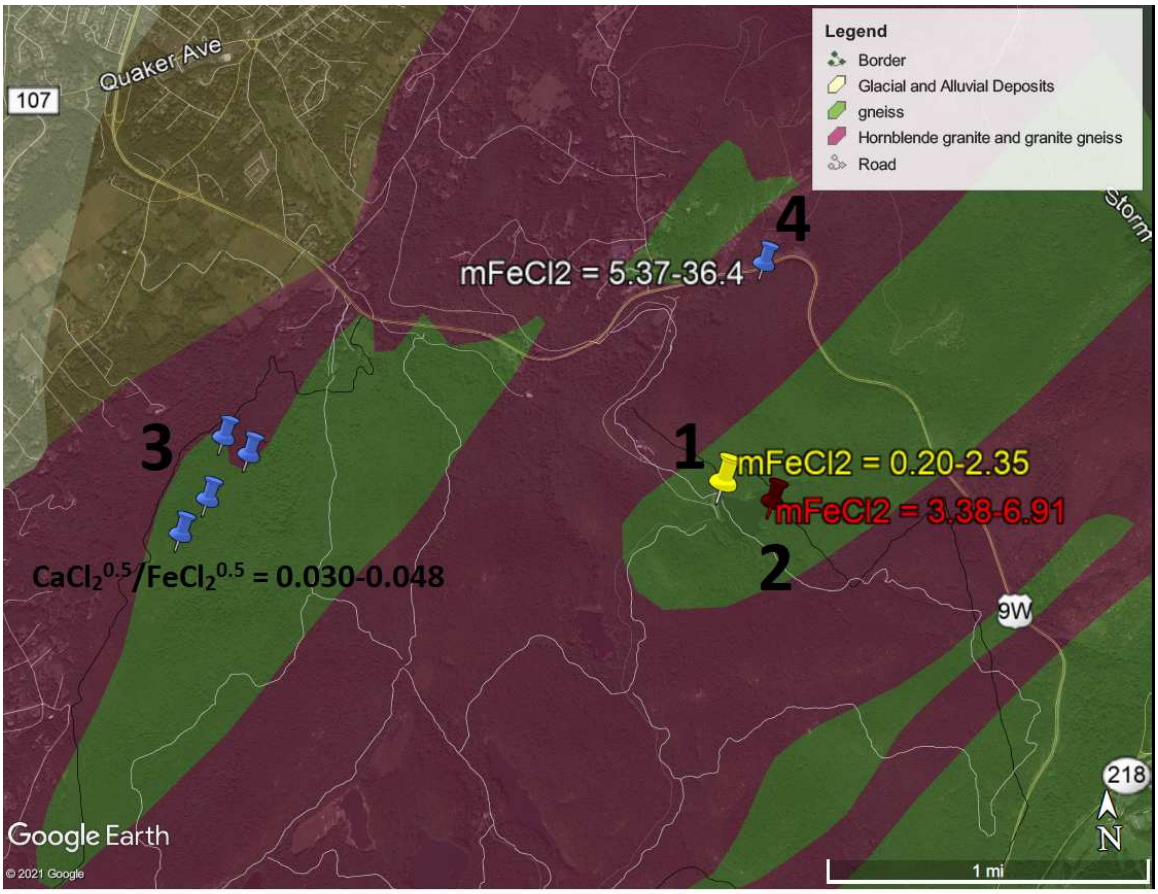


Figure 19: Geologic map of the Black Rock Forest Area with corresponding molalities of $FeCl_2$ to each location. Location 3 was an amalgamation of $CaCl_2$ and $FeCl_2$.

Conclusion

The database for thermochemical data on amphiboles has been becoming larger and more detailed, in large part thanks to Holland and Powell (2011). With more amphibole data becoming available a better understanding of metamorphic brines will also follow. The focus of this study was to come up with brand new ΔH_f, S°, and C_p terms for ideal K-Cl-hastingsite, and from this a new stability curve for the ideal amphibole was derived. Comparing this curve to a stability curve previously formed from experimental work on potassium- and chlorine-rich amphiboles (Matteucci, 2019) the ideal stability curve was offset to lower temperatures due to solid solution in the amphibole.

The exchange of halogens, such as Cl, between fluids and amphiboles have been known to occur in various geologic processes from mantle metasomatism to economic deposit formation. The Black Rock Forest in Cornwall, NY was previously mined for iron ore in the 1700s and 1800s. The gneisses that produced these iron ores also have been found to contain amphiboles with higher Cl concentrations. This made it an ideal area to apply the thermochemical data on Cl-rich hastingsite to a study of fluid-rock interactions in this area, the results of which showed a variable range of KCH activities in the analyzed amphiboles and corresponding range of mCl. This lack of uniformity across the Black Rock Forest indicates that the metamorphic brine is present in localized channels or fractures rather than as a pervasive fluid. This would agree with the earlier

study of Kusebauch et al. (2015) who found that amphibolite- to granulite-facies gneisses in the Bamble sector of SE Norway were formed from channelized flows not pervasive flows.

Further investigations into the Black Rock Forest would be a great way to understanding the fluid-rock interactions. More samples collected in more locations would also aid in determining whether these fluids were pervasive or channelized.

References Cited

Barnes, J. D., and Cisneros, M., 2012, Mineralogical control on the chlorine isotope composition 452 of altered oceanic crust: Chemical Geology, v. 326-327, p. 51-60.

Black Rock Forest Consortium, Maps, URL: www.blackrockforest.org/about/about-forest/maps (accessed August 2019).

Bowen, N. L., and Schairer, J. F., 1935, Grünerite from Rockport, Massachusetts, and a series of 458 synthetic fluor-amphiboles: American Mineralogist, v. 20, p. 543-551.

Chan, A., Jenkins, D. M., and Dyar, M. D., 2016, Partitioning of chlorine between NaCl Brines and ferro-pargasite: Implications for the formation of chlorine-rich amphiboles in mafic rocks. Canadian Mineralogist, 54, 337-351.

Comeforo, J. E., and Kohn, J. A., 1954. Synthetic asbestos investigations, I: Study of synthetic 468 fluor-tremolite: American Mineralogist, v. 39, p. 537-548.

Diener, J. F. A., Powell, R., White, R. W., and Holland, T. J. B. (2007) A new thermodynamic model for clino- and orthoamphiboles in the system Na_2O-CaO-FeO-MgO-Al_2O_3-SiO_2-H_2O-O. Journal of Metamorphic Geology, 25, 631-656.

Driscall, J., Jenkins, D.M., Dyar, D.M., and Bozhilov, K.N., 2005, Cation ordering in synthetic 472 low-calcium actinolite: American Mineralogist, v. 90, p. 900-911.

Frezzotti, M. L., Ferrando, S., Peccerillo, A., Petrelli, M., Tecce. F., and Perucchi, A., 2011, Chlorine-rich metasomatic H2O-CO2 fluids in amphibole-bearing peridotite from Injibara (Lake Tana region, Ethiopian plateau): Nature and evolution of volatiles in the mantle of a region of continental flood basalts: Geochimica et Cosmochimica Acta, c. 74, p. 3023-3039.

Frost, B. R., 1991, Introduction to oxygen fugacity and its petrologic importance. In, D. H. Lindsley, ed., Oxide minerals: petrologic and magnetic significance. Reviews in Mineralogy, Vol 25, p. 1-9.

Hawthorne, F. C., & Oberti, R., 2007, Amphiboles: crystal chemistry, *in* Hawthorne, F.C., Oberti, R., Ventura, G. D., and Mottana, A., ed., Amphiboles: Crystal Chemistry, Occurrence, and Health Issues, Volume 67: Chantilly, VA, The Mineralogical Society of America, p. 1-54.

Henry, D.J., & Daigle N.M, 2018, Chlorine incorporation into amphibole and biotite in high-grade iron-formations: Interplay between crystallography and metamorphic fluids, Volume 103: American Mineralogist, p. 55-68.

Holland, T. J. B., 2019, AX, A program to calculate activities of mineral endmembers from chemical analyses (usually determined by electron microprobe). Website: http://mill2.chem.ucl.ac.uk/ccp/web-mirrors/crush/astaff/holland/ax.html.

Holland, T.J.B., & Powell, R., 2011, An improved and extended internally consistent thermodynamic dataset for phases of petrologic interest, involving a new equation of state of solids. Journal of Metamorphic Geology, 29, 333-383.

Isachsen, Y. W., Landing, E., Lauber, J. M., Rickard, L. V., and Rogers, W. B., 2000, Geology of New York, 2nd ed., New York State Museum Educational Leaflet 28, Albany, NY, 294pp.

Jenkins, D. M., 2019, The incorporation of chlorine into calcium amphibole: American Mineralogist, v. 104(4), p. 514-524.

Kendrick, M. A., Honda, M., and Vanko, D. A., 2015, Halogens and noble gases in Mathematician Ridge meta-gabbros, NE Pacific: implications for oceanic hydrothermal root zones and global volatile cycles: Contributions to Mineralogy and Petrology, v. 170 (5), p. 1-20.

Kusebauch, C., John, T., Barnes, J. D., Klügel, A., and Austrheim, H. O., 2015, Halogen 532 element and stable chlorine isotope fractionation caused by fluid-rock interaction (Bamble 533 Sector, SE Norway): Journal of Petrology, v. 56, p. 299-324.

Léger, A., Rebbert, C., & Webster, J., 1996, Cl-rich biotite and amphibole from Black Rock Forest, Cornwall, New York: American Mineralogist, v. 81 (3-4), p. 495-504.

Locock A.J., 2014, An Excel spreadsheet to classify chemical analyses of amphiboles following the IMA recommendations, Computers for Geosciences v. 62, p. 1-11.

Makino, K., & Tomita, K., 1983, Cation distribution in the octahedral sites of hornblendes: American Mineralogist: v. 74, p. 1097-1105.

Matteucci, J. P., 2019, The effect of chlorine incorporation on the upper thermal stability of potassic-hastingsite. MS Thesis, Binghamton University, State University of New York.

Morrison, J., 1991, Compositional constraints on the incorporations of Cl into amphiboles, American Mineralogist, V. 76, p. 1920-1930.

Mueller, B. L., Jenkins, D. M., and Dyar, M. D., 2017, Chlorine incorporation in amphiboles synthesized along the magnesio-hastingsite–hastingsite compositional join. European Journal of Mineralogy, 29, 167-180.

Pavlovich, M. S., Jr., and Jenkins, D. M., 2003, Assessment of cation substitutions along the gallium and fluorine analogue of the tremolite-glaucophane join: American Mineralogist, v. 88, p. 1486-1495.

Robert, J.-L., Della Ventura, G., and Thauvin, J.-L., 1989, The infrared OH-stretching region of synthetic richterites in the system Na2O-K2O-CaO-MgO-SiO2-H2O-HF: European Journal of Mineralogy, v. 1, p. 203-211.

Robie, R.A. and Hemingway, B. S., 1995, Thermodynamic properties of minerals and related substances at 298.15 K and 1 bar (10^5 Pascals) pressure and at higher temperatures. U. S. Geological Survey Bulletin 2131, 461 pp.

Shannon, R., 1976, Revised effective ionic radii and systematic studies of interatomic distances in halides and chalcogenides: Acta Crystallographica, v. 32, p. 751-767.

Sharma, A. and Jenkins, D. J., 1999, Hydrothermal synthesis of amphiboles along the tremolite-pargasite join and in the ternary system tremolite-pargasite-cummingtonite. American Mineralogist, 84, 1304-1318.

Smith, J. R., & Hazen, R. M., 1973, The Crystal Structures of Forsterite and Hortonolite at Several Temperatures Up to 900"C: American Mineralogist, v. 58, p. 588-593.

Toby, B. H., & Von Dreele, R. B., 2013, GSAS-II: the genesis of a modern open-source all purpose crystallography software package: Journal of Applied Crystallography, v. 46(2), p. 544-549.

USGS, New York Geologic Map Data: mrdata.usgs.gov/geology/state/state.php?state=NY.

Weschler, B. A., Lindsey, D. H., & Prewett, C. T., 1984, Crystal structure and cation distribution in titanomagnetites (Fe3-,Ti,Oa): American Mineralogist, v. 69, p. 754-770.

Yardley, B.W.D., 2005, Metal Concentrations in Crustal Fluids and Their Relationship to Ore Formation: Economic Geologist, v. 100.

Zhu, C. & Sverjensky, D.A., 1991, Partitioning of F-Cl-OH between minerals and hydrothermal fluids: Geochemica et Comochimica Acta, v. 155, p. 1837-1858.

ProQuest Number: 28651190

INFORMATION TO ALL USERS
The quality and completeness of this reproduction is dependent on the quality
and completeness of the copy made available to ProQuest.



Distributed by ProQuest LLC (2021).
Copyright of the Dissertation is held by the Author unless otherwise noted.

This work may be used in accordance with the terms of the Creative Commons license
or other rights statement, as indicated in the copyright statement or in the metadata
associated with this work. Unless otherwise specified in the copyright statement
or the metadata, all rights are reserved by the copyright holder.

This work is protected against unauthorized copying under Title 17,
United States Code and other applicable copyright laws.

Microform Edition where available © ProQuest LLC. No reproduction or digitization
of the Microform Edition is authorized without permission of ProQuest LLC.

ProQuest LLC
789 East Eisenhower Parkway
P.O. Box 1346
Ann Arbor, MI 48106 - 1346 USA